The Kabua 1 cranium: virtual anatomical reconstructions

Abel Marinus Bosman[1], Laura Tabitha Buck[1,2,3], Hugo Reyes-Centeno[1], Marta Mirazón Lahr[4], Chris Stringer[3], Katerina Harvati[1,5]

[1] DFG Center for Advanced Studies 'Words, Bones, Genes, Tools: Tracking Linguistic, Cultural and Biological Trajectories of the Human Past', Eberhard Karls Universität Tübingen, Rümelinstraße 19-23, D-72070 Tübingen, Baden-Württemberg, Germany.

[2] PAVE research group, Department of Archaeology, University of Cambridge, Cambridge, CB2 3QG, United Kingdom.

[3] Centre for Human Evolution Research, Department of Earth Sciences, The Natural History Museum London SW7 5BD, United Kingdom.

[4] Leverhulme Centre for Human Evolutionary Studies, Department of Archaeology & Anthropology, University of Cambridge, Cambridge, UK.

[5] Paleoanthropology Senckenberg Center for Human Evolution and Paleoecology, Eberhard Karls Universität Tübingen, Rümelinstraße 23, D-72070 Tübingen, Baden-Württemberg, Germany.

Abstract

Our current knowledge of the emergence of anatomically modern humans, and the human lineage in general, is limited, in large part because of the lack of a well preserved and well dated fossil record from Pleistocene Africa. Thus, the primary aim of our research is to partly relieve this problem by virtually reconstructing and analyzing the hominin cranial remains of Kabua 1, found in Kenya in the 1950s. Most scholars have argued that Kabua 1 represents an anatomically modern *Homo sapiens*, although the fragmentary nature of the remains and lack of a chronometric date hinder robust phylogenetic and taxonomic assessments. This manuscript presents the first steps taken to resolve this issue, namely a set of reconstructions of the specimen that would allow comparison with the fossil record. First, we virtually removed sediment and laboratory adhesives from μCT scans of the fragments. Subsequently, all fragments were separated by segmentation of the μCT data and described. Finally, virtual surface projections were used in the creation of several anatomical reconstructions, based on separate reference crania. These first steps provide a framework that will be used for quantitative shape analyses that aim to more firmly place these remains in the context of human evolution.

Introduction

During the last few years, interest in the evolution of *H. sapiens* has increased greatly, as reflected by several scientific and popular publications (e.g. Stringer 2016; Hublin et al. 2017). However, we still have limited knowledge of the specifics of the evolution of *H. sapiens* and the emergence of a "modern" anatomy characterized by a suite of traits present, or found at high frequency, in populations living today. This is partially due to the fact that a well preserved and well dated fossil record from of sub-Saharan Africa is lacking, excluding several fossils from the Middle Pleistocene (White et al. 2003; Fleagle et al. 2008; Hublin et al. 2017) and the Late Pleistocene (Grine et al. 2007; Crevecoeur et al. 2009; Harvati et al. 2011; Tryon et al. 2015; Crevecoeur et al. 2016). Specifically, hypotheses about the emergence of diagnostic *H. sapiens* traits cannot be rigorously tested because of the limited paleoanthropological record. This gap in our current knowledge can be partially filled by reconstructing and re-analyzing known fragmentary remains. The Kabua hominin remains are critical in this regard. This material was excavated in 1959, west of Lake Turkana in Kenya, near the Kabua Gorge and consists of at least three individuals (Whitworth 1966). The material is curated by the Natural History Museum in London as part of the Palaeoanthropology collection (Buck & Stringer, 2015). Kabua 1 (K1) is the most complete individual and is represented by a fragmented calvaria, a right hemimandible, and a small right maxillary fragment. This individual is commonly considered adult (Whitworth 1966; Schepartz 1987) and possibly male (Schepartz 1987). Kabua 2 (K2) consists of several frontal fragments, while Kabua 3 (K3) is represented by a small parietal fragment. There are also two isolated molars which were found in close association with K1 (Whitworth 1966; Buck and Stringer 2015).

Even though the material from the Kabua locality is not often discussed in the palaeoanthropological literature, there has been some discourse on the K1 cranium. According to Whitworth (1966), this specimen exhibits a set of distinct features, such as thick vault bones, a receding forehead, pronounced brow ridges, an inflated glabella, and an extremely robust mandible that possesses a chin. He particularly emphasized some of these traits as "Neanderthaloid" (Whitworth 1966), a statement linked to the common idea at this time that human evolution in the Old World went through a Neanderthal phase (Hrdlička 1927, Hublin 2009). However, most other scholars have disagreed with these findings. Schepartz (1987) and Rightmire (1975) have argued that the robusticity, inflated glabella, large mandible, and presence of a chin are comparable to other Holocene *H. sapiens* specimens from eastern Africa. Additionally, Phenice (1972), Rightmire (1975), and Bräuer (1978) have reasoned that

the interpretation of a receding frontal bone and low vault is the result of the reconstruction line drawings provided by Whitworth (1966), rather than accurately reflecting the morphology of the fossil. Finally, a recent investigation of the bony labyrinth of K1 and a multivariate analysis based on ten metric variables suggested a closer affinity to anatomically modern humans than to Neanderthals (Reyes-Centeno et al. 2014). However, despite these multiple lines of evidence, there is currently no definite consensus on the taxonomic affiliation of the Kabua remains.

This manuscript will pave the way to addressing some of these issues by presenting an exhaustive description of the K1 material, which has not been undertaken since the initial publications by Whitworth (1960; 1966), together with several new virtual anatomical reconstructions. To this end, we use a suite of methods from the field of virtual anthropology or computer-assisted paleoanthropology (Zollikofer et al. 1998; Weber 2001; Zollikofer and Ponce de León 2005; Gunz et al. 2009; Weber and Bookstein 2011; Weber 2015). These methods include (1) the separation of bony material from surrounding matrix and laboratory adhevises by virtual segmentation of (μ)CT-scans, (2) generation of three-dimensional (3D) rendered models, (3) reconstructing 3D models of fragments in a virtual environment, and (4) adapting these reconstructions according to several anatomical guidelines and evolutionary hypotheses (Zollikofer and Ponce de León 2005). The benefit of using a virtual environment is that it minimizes fossil handling and thus contributes to a specimen's preservation. It also provides access to a large corpus of sophisticated exploratory and analytical tools that are otherwise unavailable. Additionally, digital data allows multiple researchers to try multiple variations on reconstructions, while also making visualizations more accessible and allowing for easy data sharing.

The aims of this manuscript are twofold. First, our evaluation of the available anatomical information will help re-contextualize the K1 material, as general knowledge of Middle/Late Pleistocene hominins has increased greatly since the 1960s. Second, through the use of several virtual techniques, we intend to gain new information on the Kabua 1 cranium. These preliminary results, together with a detailed description on how we approached the reconstruction of this cranium, will aid us in our future quantitative analyses of the taxonomic affiliation of this specimen when a chronometric date can be determined.

The Kabua material – Historical and archaeological context
On 8 September 1959, a team of geologists led by Thomas Whitworth from the University of Durham, discovered two localities containing skeletal material on the western shore of Lake

Turkana in Kenya (Whitworth 1960). The remains were excavated from lake sediments on the eastern flank of the Lothidok Hill range, immediately south of the Kalokol River and near the Kabua Gorge, approximate position 35° 47´E., 3° 26´ N. (Whitworth 1960). The material was located near a watering hole referred to as 'Kabua' by the research team and as 'Kadokorinyang' by the local people (Shea and Hildebrand 2010). K1 was found about 1 km SSE from the Kabua watering hole, while K2 and K3 were found at an unreported distance from K1, but a measurement on a published map (Whitworth 1965a) yields an approximate distance of 1200 meters.

There is much uncertainty about the actual antiquity of the Kabua remains. According to Whitworth (1965a), the matrix encasing the hominin remains was of Late Pleistocene antiquity, as determined by Arambourg et al. (in Whitworth 1965a) and Fuchs (1934) on the basis of mollusks and faunal remains (Whitworth 1960, 1965a, 1965b; Whitworth 1966; Buck and Stringer 2015). However, Owen et al. (1982) argue that these lake sediments are part of a larger complex of deposits, known as the Galana Boi Formation, and regard them as early- to mid-Holocene in age. Moreover, oral tradition and archaeological evidence suggest that the faunal remains belonged to animals that survived in this area until recently (Robbins 1972).

Attempts at establishing a chronometric context for the Kabua remains have had limited success. Uranium and fluorine relative dating carried out by Kenneth Oakley at the Natural History Museum, London were inconclusive (Buck and Stringer 2015). Shells from a layer ~15m above the base of the Kabua lake beds were radiocarbon dated to between 5500 and 7500 years BP (Buck and Stringer 2015). While no directly associated artifacts were found *in situ* with the hominin remains, a stone tool assemblage was recovered from the surface near the Kabua lake beds. This assemblage included artifacts that Whitworth (1965a) referred to as consisting of Kenya Stillbay lithics, Upper Kenya Capsian microliths, and some Sangoan handaxes. Whitworth (1965a) reported that the Sangoan handaxes, which were possibly derived from a horizon that overlay the Kabua skeletal material, were ascribed to the Early, Middle, and Late Sangoan industries by independent specialists, although names of these specialists were not given. Additionally, none of these handaxes have been figured or described in detail. Moreover, the so-called Kenya Stillbay and Upper Kenya Capsian industries, the latter of which has been later partly redefined as Eburran (Ambrose 1980; Wilshaw 2016), are generally considered to be Middle and Later Stone Age, respectively. Since the handaxes come from distinct archaeological periods and there is a hiatus of several thousand years in between the Stillbay and Eburran industries, it is possible that there has been substantial stratigraphic mixing at the entire Kabua locality. Furthermore, assigning

exact dates to broad periods such as the MSA is problematic, as MSA industries occur at different points in time throughout the continent, with the added factor that new sites are being uncovered every year. For example, the oldest MSA-bearing site in eastern Africa as currently considered is in the Olorgesailie Basin, Kenya, dated to around 320 ka (Deino et al. 2018). Several years ago, the oldest MSA-bearing site was part of the Gademotta complex, which was argued to be older than 280 ka (Morgan and Renne 2008; Sahle et al. 2013), showing how our understanding of the chronology of this industry is changing rapidly. Moreover, several scholars (e.g. Blegen et al. 2017 and Tribolo et al 2017) present evidence of MSA technology at sites in eastern Africa that are younger than 36 ka. This variability precludes the use of lithic technologies in securely dating archeological contexts. In an attempt to resolve the dating issues associated with the Kabua material, direct dating of the hominin remains is currently underway with ESR and U-series methods (Buck and Stringer 2015).

Materials and Methods

The fragments of the K1 cranium were scanned in six segments with a Nikon Metrology HMX ST 225 μCT machine, located at the Natural History Museum in London (Fig. 1, Supplementary Table 1), with parameters optimized for the variable sizes, densities, and states of mineralization (Table 1).

Table 1. Parameters used for the scanning of the six segments. All filters were copper.

Segment	Museum Index	Voltage (kV)	Power (mA)	Filter thickness (mm)	Number of slices	Pixel size (μm)
Posterior calvaria	EM2468	215	200	2	1890	0.096
Frontal	EM2469	180	150	0.5	1520	0.083
Left temporal	EM2470	200	165	1	1256	0.083
Right temporal	EM2471	135	200	0.5	1102	0.0427
Mandible	EM2480	210	175	2	1772	0.0863
Maxilla	EM2481	190	175	1	1654	0.0236

Subsequently adhesive, plaster, and sediment were virtually removed in Avizo Lite 9.0.1 (FEI Visualization Sciences Group, using manual and semi-automatic segmentation based on thresholding and region growing. Some fragments, especially the fragments of the

right temporal bone, are so heavily mineralized and affected by expanding matrix distortion that it was impossible to securely distinguish bone from sediment, which made subsequent estimation of anatomical features unreliable. Therefore, these fragments (EM2471) were not included in the anatomical reconstructions. Surface models were extracted after segmentation and together with high quality photographs of the K1 material, were used to describe each fragment and any recognizable anatomical features. In order to standardize our observations of several non-metric traits (Supplementary Table 2), we used the scoring systems compiled and published by Buikstra and Ubelaker (1994).

To reassemble the calvaria, we used evidence of direct articulation, anatomical features, and geometric similarities of fracture surfaces wherever possible. This follows general best practice, which dictates that one should rely on the morphological information obtained from the fossil(s) in question (Zollikofer and Ponce de León 2005). Articulation between fragments was independently assessed by three of the authors (AB, HRC, and LTB) and fragments were only fixed in place when a consensus was reached. To reassemble the non-articulated fragments, extrinsic information was employed to locate and register 'floating' fragments in an anatomically sensible location. This process relies on inference based on symplesiomorphic crania (Weber and Bookstein 2011). However, since the K1 cranium purportedly displays a mix of plesiomorphic and autapomorphic features, and the possible range of antiquity is quite large, it was deemed necessary to use a variety of possible crania in order to explore different scenarios, a practice that is common in virtual anthropology (Weber and Bookstein 2011). The crania used in this manuscript were selected for their state of preservation, diverging morphologies, geographical location, possible peri-contemporaneity with Kabua, and availability of CT scan data. These reference crania include Broken Hill (Kabwe), Ngaloba LH18, Skhūl 5, Mumba X, Masai 3 and Masai 10 (Table 2). We used these crania as a general framework to position the fragments of K1, without relying overly on the degree of similarity between the K1 fragments and the reference crania. That is to say, we prioritized the articulation between the Kabua fragments over direct superimposition of the fragments on the reference crania, in order to prevent a substantial bias towards the reference. By using the reference sample presented in Table 2, we aimed to capture a significant amount of possible variation with the data available to us. To determine whether our reconstructions are robust, in a future study we will use a set of geometric morphometric analyses that includes a larger comparative sample. Additionally, this comparative sample will be expanded to include less complete crania by, for example, limiting the quantitative analyses to specific areas of the cranium.

The following protocol was used for the superimposition of the K1 fragments on the reference. First, we manually aligned the posterior calvaria of K1 (EM2468) to the reference cranium by using the occipital superstructures (external occipital protuberance, asterion, cruciform eminence, superior nuchal lines, and parietal notch). Then, we manually aligned the frontal of K1 (EM2469) with the reference by using the frontal crest, glabella and the supraorbital margins. The posterior of the frontal was rotated until it attained a smooth curvature with the posterior calvaria. The fragments of the left temporal (EM2470) were aligned to the posterior calvaria and the frontal by estimating the position of the coronal sutures and using the smooth outline in *norma frontalis* and *norma lateralis*. The K1 maxilla (EM2481) was aligned manually to the reference, while using the frontal of K1 as a guideline. The mandible (EM2480) was aligned to the maxilla by using dental occlusion and the estimated position of the mandibular fossa on the left temporal bone.

This procedure was repeated for all reference crania. Thus, we created several distinct anatomical reconstructions, each based on a different phylogenetic and chronological scenario. However, each reconstruction was not entirely biased by the choice of reference, as smooth continuation of fragments and symmetry of the K1 cranium were favored over direct articulation with the reference crania. At the same time, using a reference-based approach ensures reproducibility by limiting the degree to which individual fragments can be spatially manipulated. In order to test the anatomical cohesion between the reconstructions and the references, we created several surface deviation models (Fig. 6; Supplementary Figs. 11-15) in Avizo, using the surface distance module, that display the amount of surface overlap between two objects by calculating the minimal distance between them. It has to be noted here that the Ngaloba LH18 reference cranium consists of two separately scanned fragments, the calvaria and the splanchnocranium, which had to be manually reconstructed. As described in the original publication of this specimen (Day et al. 1980), there is no direct anatomical articulation between these fragments and the reconstruction must therefore remain speculative. We nevertheless approximated the original reconstruction by Day et al. (1980) and note that the degree of facial prognathism can otherwise vary depending on the positioning of the splanchnocranium relative to the calvaria. In addition, the LH18 cranium is somewhat distorted in the frontal/facial area. These limitations of the reference might result in some uncertainty associated with the reconstruction of K1.

To investigate the form of the dental arcade of K1, we applied a specific mirroring protocol. In this procedure, we used a set of semilandmarks to compute a plane of symmetry at the area medial to the first incisor. Subsequently, we duplicated the original fragment and

reflected it along the artificially created plane of symmetry; a procedure that has been described by several authors (Gunz et al. 2009; Weber and Bookstein 2011). This mirrored copy of the maxilla was registered to the original fragment by using landmark surface registration with rigid transformation (Supplementary Fig. 1). However, points to define the mid-sagittal plane are only located in the most anterior portion of the maxilla, which makes the reconstruction of the dental arcade uncertain. The same procedure was applied to mirror the mandible.
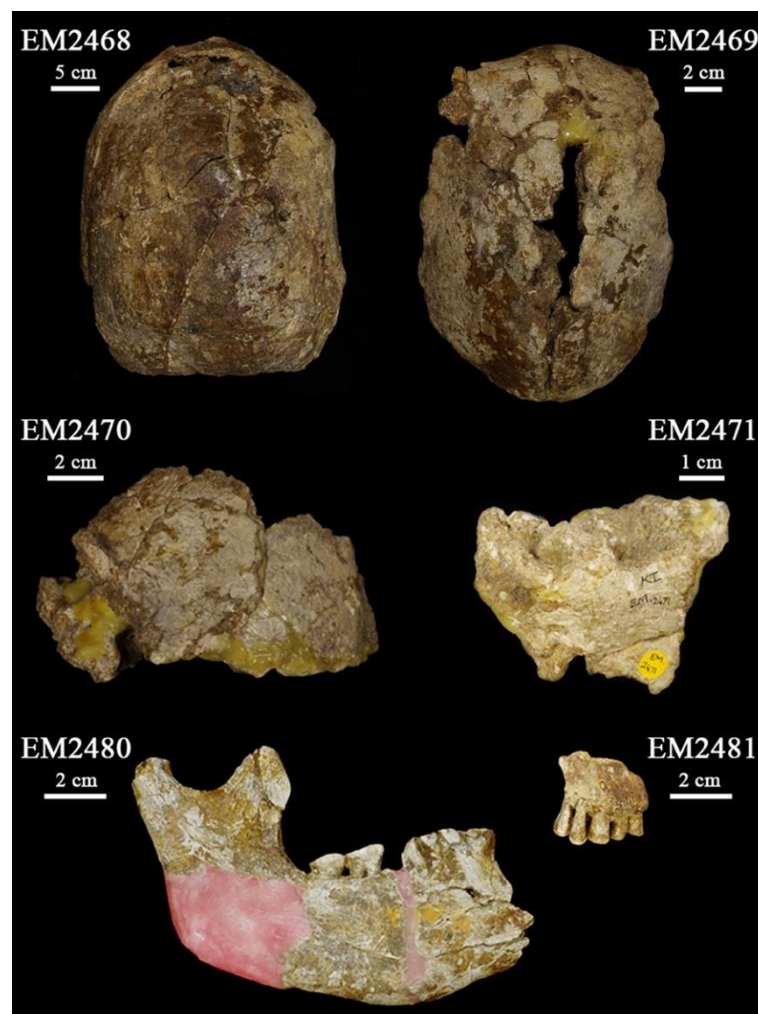
Figure 1. Selection of Kabua 1 cranial fragments. Top-left: occipital and parietals in *norma occipitali*s; top-right: frontal bone in *norma verticalis*, anterior faces up; middle-left: left temporal with petrous portion and parietal fragment in lateral view, with anterior facing up; middle-right: right temporal bone in inferolateral view with anterior facing left; bottom: preserved right hemimandible and maxillary fragment in buccal view, anterior facing right. Photographs courtesy of the Natural History Museum, London.

Table 2. Summary of comparative specimens used in the anatomical reconstructions and their proposed antiquity.

Specimen	Broken Hill	LH 18	Skhūl V	Mumba X	Masai 3 & Masai 10
Locality	Kabwe, Zambia	Laetoli, Tanzania	Skhūl Cave, Israel	Mumba rockshelter, Tanzania	Lake Eyasi region, Tanzania
Taxon	*H. heidelbergensis* s.l.	early *H. sapiens*	early *H. sapiens*	recent *H. sapiens*	recent *H. sapiens*
Antiquity	300 - 250 ka	490 – 121 ka	130 – 100 ka	>5 ka	Holocene; ~200 ya
Dating method	ESR, U-series	Thorium & Protactinium dating on giraffe vertebra	ESR, U-series	Minimum radiocarbon based on stratigraphically superior burial	Uncalibrated radiocarbon on charcoal found in grave of Masai 1
References	Buck and Stringer (2015); Balzeau et al. (2017)	Hay (1987); Millard (2008)	Grün et al. (2005)	Mehlman (1979)	Bräuer (1983)
Location†	NHML	NMT/VAV	PMH	EKUT	EKUT

† NHML = National History Museum, London, NMT = National Museum Tanzania, VAV = Virtual Anthropology Vienna, PMH = Peabody Museum, Harvard University, Cambridge, EKUT = Eberhard Karls University of Tübingen

The Kabua material – Inventory and description of the fragments

The K1 material (Figs. 1-2, Supplementary Table 1) has been described to some extent by Whitworth (1960; 1965b). In this manuscript, we summarize these descriptions and add information where needed or where we differ from Whitworth's findings.
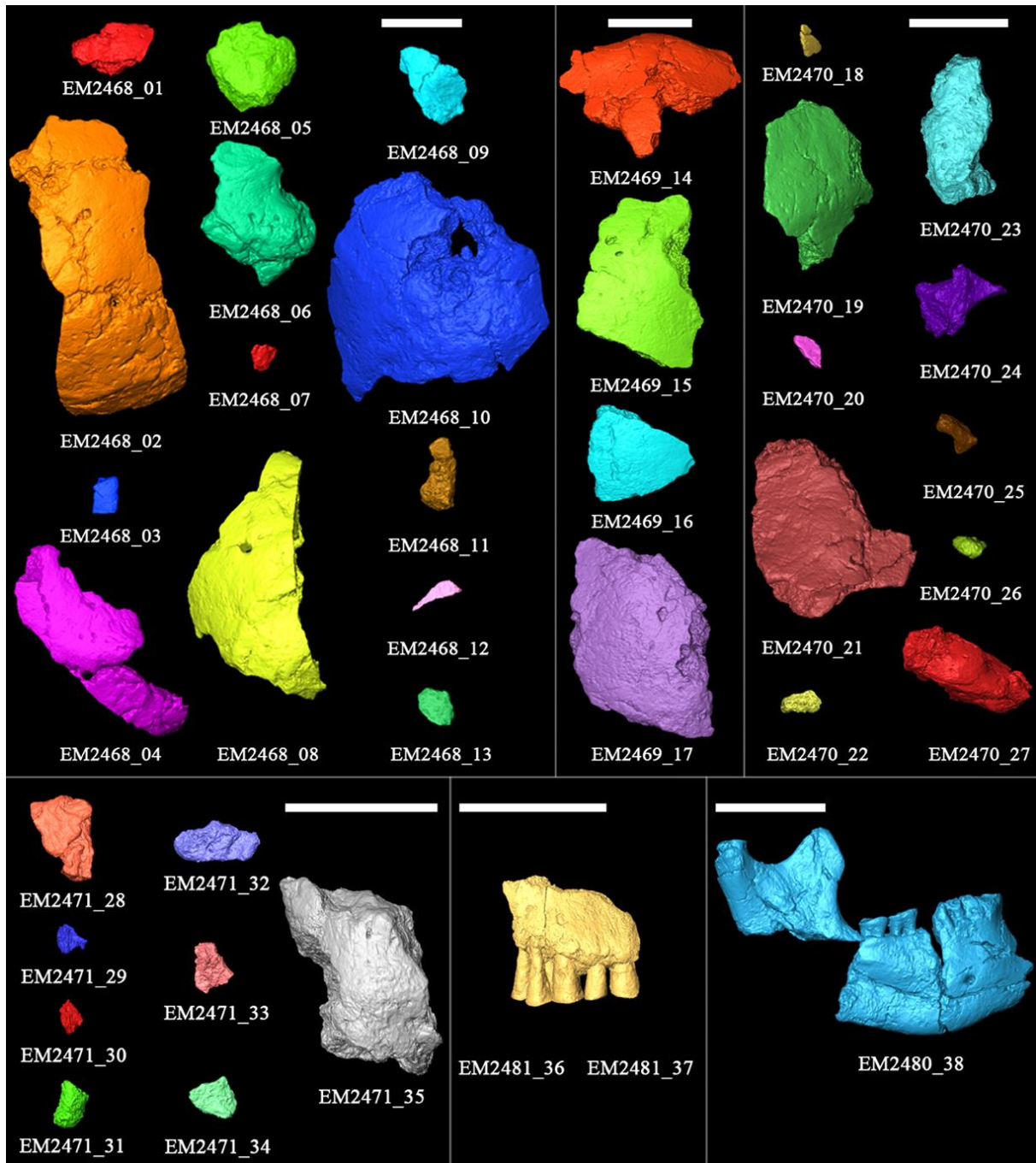
Figure 2. Inventory of the Kabua 1 remains as surface reconstructions. For EM2468, EM2469, EM2470, and EM2471, the ectocranial surfaces are facing the viewer and the anterior sides are facing up. For EM2480, the buccal side is facing the viewer, with anterior facing right. For EM2481, the anterior side is facing the viewer and superior sides face up. Labels as in Supplementary Table 1 (scale bars = 5 cm).

Occipital bone (EM2468)

The occipital squama is preserved up to a point behind opisthion, while the basilar occipital is absent (Whitworth 1966). The lambdoid suture is visible on the right side, where it is distorted

by taphonomy, and the external table is degraded. This distorts the articulation with the posterior temporal bone, EM2468_06. In the area of lambda, the lambdoid suture can only be faintly traced on the left half of the occipital plane. The occipital does not project posteriorly below lambda. The superior nuchal lines are robust and extend laterally towards asterion. There is a medial thickening present on the superior nuchal lines, but the external occipital protuberance is not pronounced; its inferior border is rounded and does not extend inferiorly of the superior nuchal lines (score 1; Buikstra and Ubelaker 1994). The cruciform eminence and transverse sulci are also not pronounced. The cerebellar fossae are of similar size as the cerebral fossae, although most of the basilar portion is not preserved. The neurocranium is high and medio-laterally compressed, partially due to taphonomic processes.

Approximately nine millimeters above the superior nuchal lines, there is a shallow oval depression, with uneven borders, that has a maximum extension in the transverse direction. It does not correspond to the suprainiac fossa commonly described for Neanderthal specimens, which are discrete, elliptical depressions with an uneven floor that extend laterally between the bilateral aches of an occipital torus (Hublin 1978; Santa Luca 1978; Balzeau and Rougier 2010). Moreover, its external surface is not characterized by localized rugosity and pitting, but is instead marked by macroscopic dents and abrasion of the external table of the cranial vault, suggesting that the depression may be the result of extensive taphonomic processes. Moreover, when analyzing a μCT slice that crosses the maximum vertical extent of the depression on K1, it is clear that only the external table is influenced (Supplementary Fig. 2). The diploë is not affected by the presence of the depression. This pattern corresponds to suprainiac depressions found in *H. sapiens* and contrasts with that observed in the Neanderthal suprainiac fossa (Balzeau and Rougier 2010).

Frontal bone (EM2469)
The frontal bone is fairly complete and consists primarily of the medial segments of the superciliary arches, the area surrounding glabella, and most of the posterior frontal bone. It is damaged around the area of the frontal suture by a long fissure that originates behind the position of glabella and separates the frontal nearly in two distinct halves. According to Whitworth (1966), this suggests imperfect metopic suture closure at the time of death. While some traces of the metopic suture persist superior of nasion in most known cases of metopism (Ajmani et al. 1983), metopic sutures of the partial type can either extend upward from nasion or downward from bregma (Zdilla et al. 2018). Moreover, the prevalence of metopism varies among different populations and sexes (Ajmani et al. 1983; Zdilla et al. 2018). In K1, the

taphonomic damage extends from the area of bregma but does not reach the area around glabella or the post-toral sulcus. However, it is also possible that the frontal bone fissure is exclusively caused by postmortem taphonomic processes. As there is no conclusive evidence for metopism, we consider the latter a more conservative interpretation. Endocranially, the frontal crest is broken off just as it bifurcates into the sagittal sulcus.

Both supraorbital margins are present to some extent, with the left being better preserved than the right (Whitworth 1966). Neither margin shows supraorbital notches, but the areas where these should be present are not fully preserved. The supraorbital margin seems fairly sharp and minimally expressed (score 2; Buikstra and Ubelaker 1994). Similarly, glabella and the supraorbital ridge are also minimally expressed (score 1; Buikstra and Ubelaker 1994). There are no clear signs of post-toral sulcus or postorbital constriction. The lateral parts of the supraorbital region are differentiated from the medial segment—a condition that is often described as anatomically modern and differs from the continuous supraorbital morphology seen in Neanderthal specimens (Smith and Ranyard 1980; Harvati et al. 2007). According to Whitworth (1966), the frontal bone of K1 displays pronounced median frontal keeling. However, this median frontal keeling seems to be mainly caused by a slight mismatch between the anterior (EM2469_14) and posterior (EM2469_15, EM2469_16, and EM2469_17) fragments in the original manual reconstruction. After positioning the fragments so that there is direct articulation between EM2469_14 and the posterior frontal fragments (right: EM2469_15, left: EM2469_17), the pronounced sagittal keel is reduced significantly (Supplementary Fig. 3).

Parietals (EM468 & EM2470)

The left parietal is better preserved than the right, although most of the anterior portion is missing, especially around bregma and posterior to the left orbit. There is a hint of a weak parietal eminence on the left parietal. The right parietal is missing a large anterior portion and is damaged by perforations near the midsagittal plane (Whitworth 1966). On the right side, the area where the parietal eminence would be located is not fully preserved and distorted by post-depositional processes. There does seem to be a trace of the posterior portion of the inferior temporal line on the right parietal (EM2468_05). The coronal suture is not preserved on either parietal bone.

Temporal bones (EM2470)

Most of the squamous portion of the left temporal is intact, including the petrous portion. While the petrous portion is displaced inwards, it is generally well preserved, which allowed for the reconstruction of the bony labyrinth (Fig. 3; Reyes-Centeno et al. 2014). The proximal portion of the postglenoid process is intact. Also present is the posterior base of the zygomatic process. The glenoid fossa, entoglenoid process, zygomatic process, parietal notch, and most of the tympanic plate are not preserved. Concerning the mastoid process, the ectocranial surface is damaged. On the right side, only the posterior aspect of the temporal bone is present, which includes the mastoid process and a fairly pronounced supramastoid crest. While it is quite broad, the mastoid processes do not extend inferiorly (score 2; Buikstra and Ubelaker 1994). Concerning the right temporal bone, Whitworth (1966) only describes the posterior aspect. However, the K1 material includes a very heavily mineralized fragment catalogued as a squamous portion of a right temporal bone (EM2471). This fragment includes the articular eminence and the mandibular fossa but the presence of these features cannot be established with much certainty, as the entire temporal is afflicted by expanding matrix distortion (Fig.1), which makes an accurate assessment of its anatomical features extremely difficult. However, as far as can be determined, the tympanic part, petrous portion, and other diagnostic features such as the styloid process or the auditory meatus are not preserved.

While most of basilar calvaria is not preserved (Whitworth 1966), the distal portion of the left greater wing of the sphenoid articulates with the left temporal bone (EM2470_21 and EM2470_23; Fig. 2). On the right side, there is a singular fragment that resembles the inferio-distal part of the right greater wing (EM2471_32), but this assessment cannot be determined with certainty due to the extensive expanding matrix distortion, as earlier described for the right temporal.
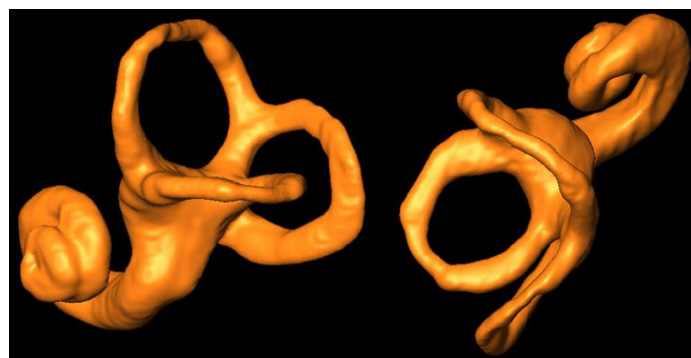

Figure 3. Reconstruction of the Kabua 1 left bony labyrinth in lateral (left) and superior (right) view.

Mandible (EM2480)

The right hemi-mandible is well preserved, as most of the right sigmoid sulcus, inferior portion of the articular condyle, coronoid process, mandibular ramus, and mandibular corpus are present. Just behind the second premolar, the mandible is almost completely separated into two pieces, but the inferior border and adhesives from Whitworth's reconstruction hold the two fragments together. The gonial area is reconstructed as well. There is some post-depositional deformation in the form of a large oval depression on the buccal side of the mandibular corpus, inferior to the first and second molars (Figs 1 & 2). Overall, the corpus of the mandible is robust, primarily in the lingual area, which is dominated by a mylohyoid ridge that develops into a pronounced mandibular torus. The mandibular corpus has been described as deep by Wood (2011). Moreover, Whitworth (1966) and several other authors (e.g. Schepartz 1987; Wood 2011) have argued that there is an unequivocal presence of a chin. While there is a posteriorly oriented slope between the alveolar process around the first incisor and the area where the mental protuberance would be located, there is not sufficient bone preserved to ascertain the exact morphology of this area. Behind the third molar, there is a narrow space that Wood (2011) describes as a retromolar gap. The retromolar gap is commonly referred to as a Neanderthal autapomorphy (e.g. Stringer et al. 1984; Franciscus and Trinkaus 1995; see also Harvati 2015) and has been related to processes such as mid-facial prognathism (Rak 1986; Rosas 2001) and a decrease in size of the buccal teeth (Brace 1979). However, Rosas and Bastir (2004) and Nicholson and Harvati (2006) found that the retromolar gap was related to increasing mandibular size and is not autapomorphic for *H. neanderthalensis*. Thus, there is some uncertainty regarding the Neanderthal derived status of the retromolar gap, and the narrow space behind the third molar in the K1 mandible might simply be related to the relative large size and robusticity of the mandibular corpus and its comparably small dentition.

The K1 lower dentition (I_2 to P_4, M_2, and M_3) is heavily worn and the enamel is mostly abraded. While most of the traits present are common in *H. sapiens* (i.e., smaller bucco-lingual diameter of the first molar when compared to the second molar, vertical lingual wall versus an inflated buccal wall), Whitworth (1966) notes that the roots of the second lower molar seem to consist of two external roots and one, "pillar-like" median internal root. Similarly, he argues that the third molar only presents a singular fused root (Whitworth 1966). He equates these structures to the enlarged pulp chambers in molars, taurodontism, found in the Neanderthal dentition from Krapina (Whitworth 1966). While taurodontism is more common in Neanderthals, it is also found in varying frequencies in Late Pleistocene *H.*

sapiens (Kupczik and Hublin 2010). However, while the external morphology of the roots is unclear due to the presence of sediment, a series of ortho slices show that both M_2, and M_3 possess two major external roots with an early invagination (Supplementary Fig. 4), a condition typical for *H. sapiens* (Kupczik and Hublin 2010).

Maxilla (EM2481)

The maxilla is represented by a small fragment of the right medial alveolar process and is heavily damaged around the midline. In general, the labial surface of the alveolar process is quite flat and not pronounced. There is no evidence of a pronounced naso-alveolar clivus. Likewise, what is preserved of the palate is not robust. There is no evidence of a greater palatine groove, although most of the area where this structure would be located is not preserved. In contrast to what has been stated by Whitworth (1966), not enough of the maxilla is preserved to securely estimate the position of the anterior root of the zygomatic arch, nor of the presence of a canine fossa.

After reflection of the maxilla along the sagittal plane, the dental arcade has a parabolic, semi-circular appearance (Supplementary Fig. 1). The incisors, canine, and premolars (I^1 to P^4 along the dental row) are preserved, although heavily affected by abrasion. The anterior teeth are particularly small (Schepartz 1987). As with the mandibular dentition, most of the enamel has degraded due to abrasion, especially on the lingual side of the incisors, where the cervical margin has completely worn away. On the labial side, the proximal portion of the cervical margin is still present, primarily on P^3 and P^4.

Results & Discussion

While we used several morphologically distinct reference crania in the virtual reconstruction of K1, there is an overall consistency between the reconstructions in regards to general cranial shape. (Figs. 4-6, Supplementary Figs. 5-15). All anatomical reconstructions present fairly globular crania—a hallmark trait of anatomical modernity (Pearson 2008; Gunz et al. 2012; Neubauer et al. 2018), which could be established with some confidence, as the preserved cranial vault is located fairly close to the frontal bone. Moreover, the anatomically correct curvature between the frontal and temporal sections on the left side is preserved to some extent, even though direct articulation could not be established. The reconstructions are at their widest in the mid-parietal region, and do not present a posterior extension of the occipital squama—a feature that is present on the Broken Hill cranium. Moreover, the K1 fragments are not as robust as the Skhūl V cranium but seem to be quite gracile and more

comparable to the Masai 03 and Masai 10 individuals. In addition, some of the cranial traits present on K1 (nuchal crest, mastoid process, supraorbital margin, and glabella) were found to be minimally expressed. This might signify that the K1 cranium was female, rather than male, as suggested forward by Schepartz (1987). However, the lack of other skeletal elements, such as the pelvis, that can contribute to the estimation of sex precludes a definitive assessment.

Overall, the recent *H. sapiens* reference crania (Fig. 6; Supplementary Figs. 8-10, 14-15) result in reconstructions that have the most anatomical cohesion, together with the reconstruction based on Skhūl V. In these reconstructions, the fragments of K1 align well to the frontal, the anterior portion of the parietals, and the superior of the occipital bone. The posterior protrusion of the occipital bone overlaps the most with its reference in the reconstruction based on Masai 03 (Fig. 6) It should be noted that in all reconstructions, the surface deviation models highlight that the lower scale of the occipital and inferior portions of the temporal bones of K1 extend further than the references used here. When comparing all reconstructions, the specimens with fewer anatomically modern traits (specifically Broken Hill and LH18) do not display as great a degree of anatomical cohesion as the reconstructions based on Skhūl V, Mumba, Masai 03, and Masai 10. In particular, the reconstruction based on Ngaloba LH18 is problematic. In this reconstruction, the orientation of the K1 frontal does not align well with the frontal of LH18. Furthermore, the left temporal/parietal portion does not form a smooth continuation of the coronal outline between the posterior calvaria and frontal bone. This can be partially explained by the fact that the LH18 specimen shows some degree of taphonomic deformation (see above), which likely contributes to the final reconstruction. Likewise, the reconstruction deviates from Broken Hill in very specific areas, such as the medial part of the frontal and around the position of lambda. However, since a qualitative assessment of the robustness of the reconstructions and anatomical cohesion displayed by the surface deviation models is limited in usefulness, we will use geometric morphometrics in a future study in order to better evaluate the results presented here.

As stated in the materials and methods, the reference crania were used as frameworks to correctly register fragments of K1, after inherent anatomical guidelines and articulation were exhausted. Therefore, in some of the reconstructions, there are slight mismatches between the reference cranium and the K1 fragments. This is especially evident in the reconstructions based on Broken Hill, Ngaloba LH18 and Skhūl V. Particularly troublesome was the placement of the left temporal/temporal section and the reconstruction of its relationship with the frontal. This was even more true for the maxilla and mandible. As the glenoid area in K1 is not preserved, we had to rely on the occlusion between the upper and

lower dentition to position the mandible. Due to the significant amount of dental abrasion, this placement is uncertain, which results in a large amount of variation in this area between reconstructions. Additionally, in all reconstructions K1 seems to be more inferiorly extended in the occipital and temporal regions (Figs. 4-6). This is exemplified by the especially inferiorly located temporal bone and the long nuchal crest. Moreover, all reconstructions of K1 are quite narrow at the temporo-parietal area. This is primarily caused by post-mortem distortion of the lateral right parietal/temporal region, which caused the fragments EM2468_05 and EM2468_06 to be moved medially, as well endocranially distorting a small area superior of where the temporal line should be. In our reconstructions, we have attempted to remedy this distortion by moving the EM2468_05 and EM2468_06 laterally, relative to the superior right parietal fragments. However, most of the distortion could not be solved by manually positioning fragments according to a framework; another solution should be sought for this problem.

Finally, our reconstructions present a severe limitation of the methodology that was applied. Since there is no direct articulation between the cranial vault, temporal, frontal bone, and the maxilla and mandible, these sections could be placed with several degrees of freedom and still result in anatomically viable reconstructions. Since data interpolation methods, such as thin plate spline warping, rely on the correct initial placement of the available fragments, we are unable to apply them to K1 in order to create reconstructions that would resemble what the specimen would have looked like just after deposition. This is a limitation we cannot easily overcome. In addition, we have not considered how size and allometric effects on cranial shape in our reference crania might influence our reconstructions (Mitteroecker et al. 2004; Freidline et al. 2012; Mitteroecker et al. 2013). Such limitations highlight the need to employ a widely diverging range of reference crania, as well as the creation of several reconstructions, instead of treating a certain reconstruction as the "true" form of the K1 cranium.
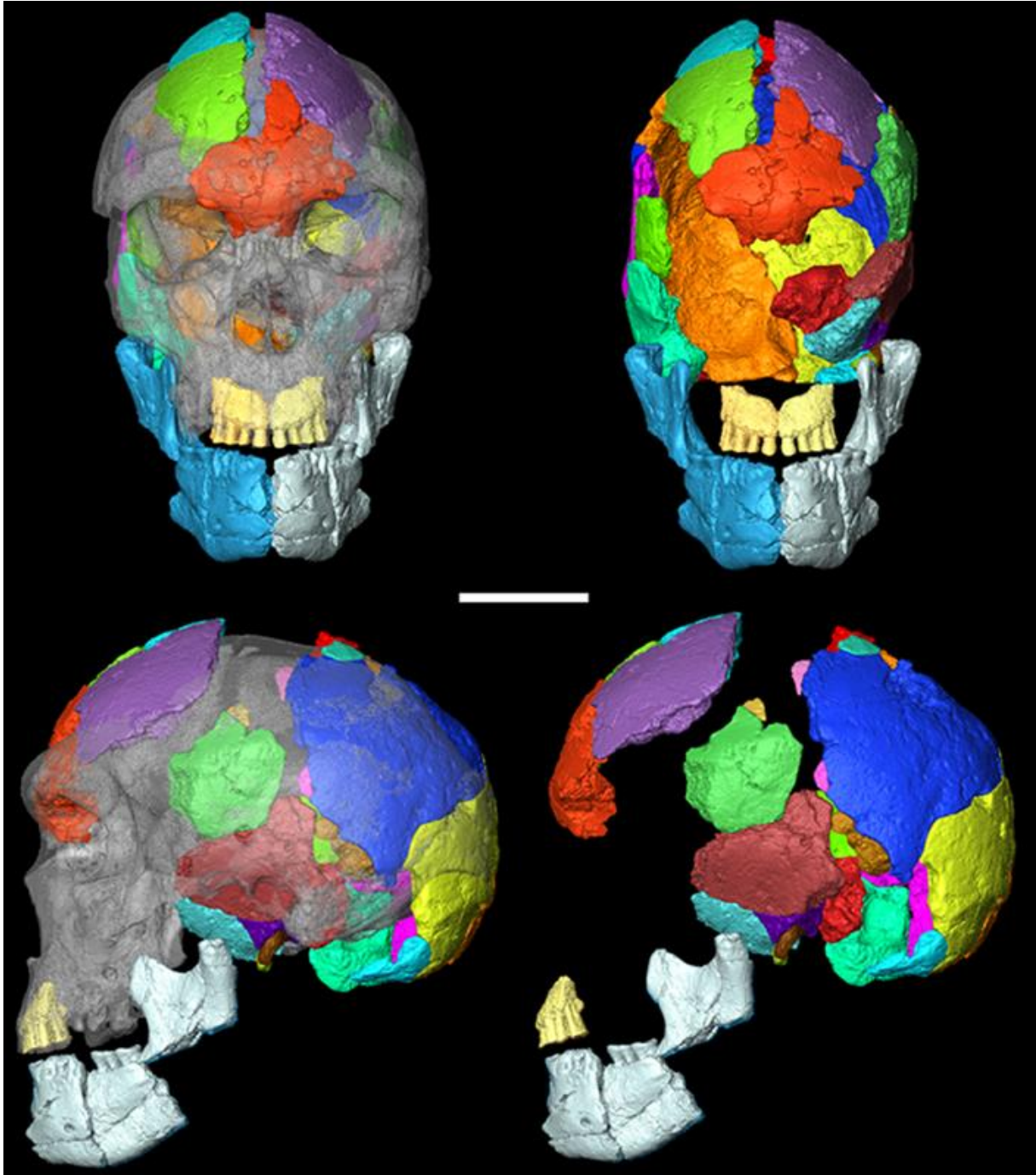
Figure 4. Reconstruction of Kabua 1, with Broken Hill as the reference. Top-left: *norma frontalis* with Broken Hill superimposed; top-right: *norma frontalis*; bottom-left: *norma lateralis sinister* with Broken Hill superimposed; bottom-right: *norma lateralis sinister* (scale bar = 10 cm). For more orientations, see Supplementary Fig. 5.
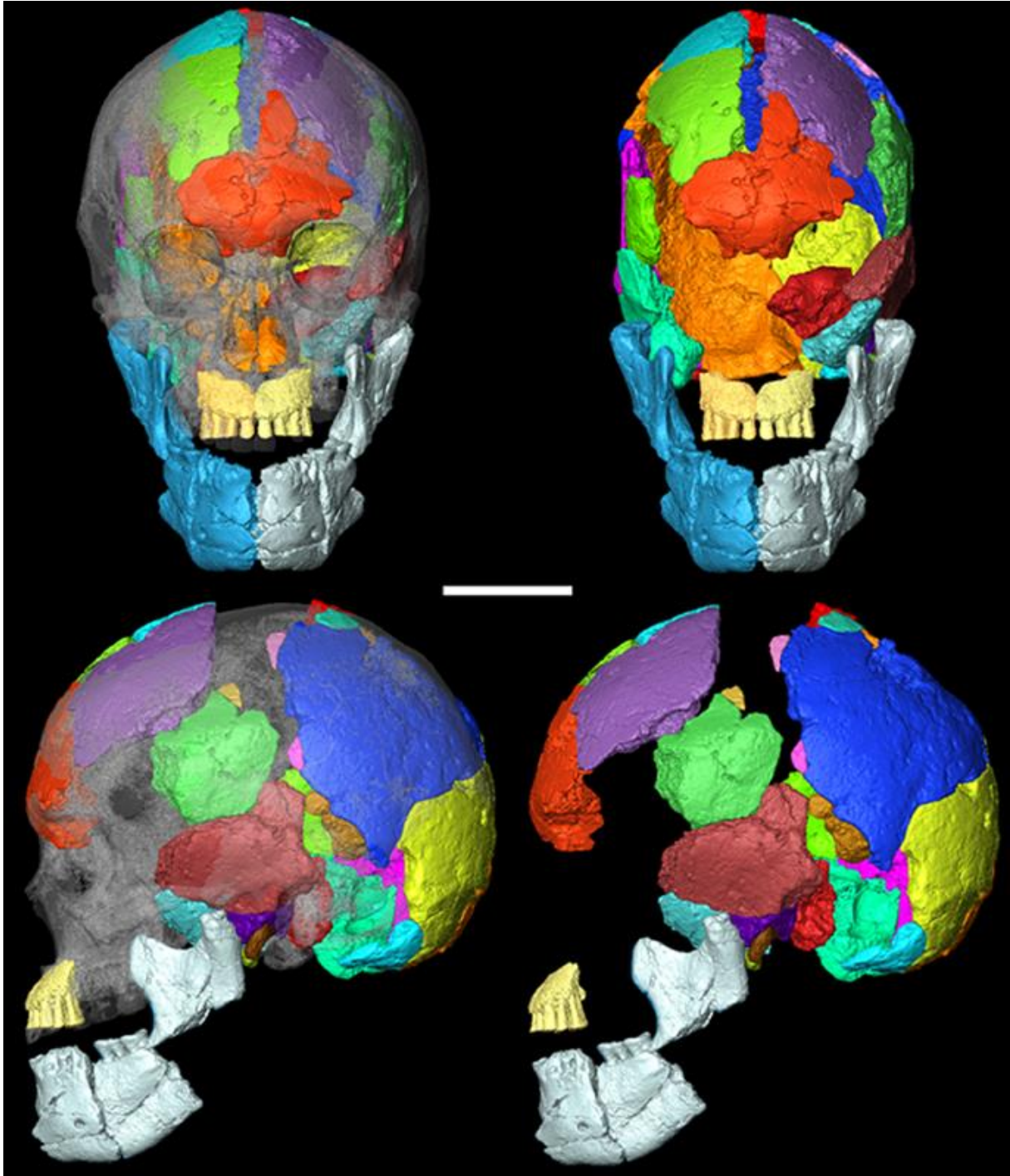
Figure 5. Reconstruction of Kabua 1, with Masai 10 as the reference. Top-left: *norma frontalis* with Masai 10 superimposed; top-right: *norma frontalis*; bottom-left: *norma lateralis sinister* with Masai 10 superimposed; bottom-right: *norma lateralis sinister* (scale bar = 10 cm). For more orientations, see Supplementary Fig. 10.
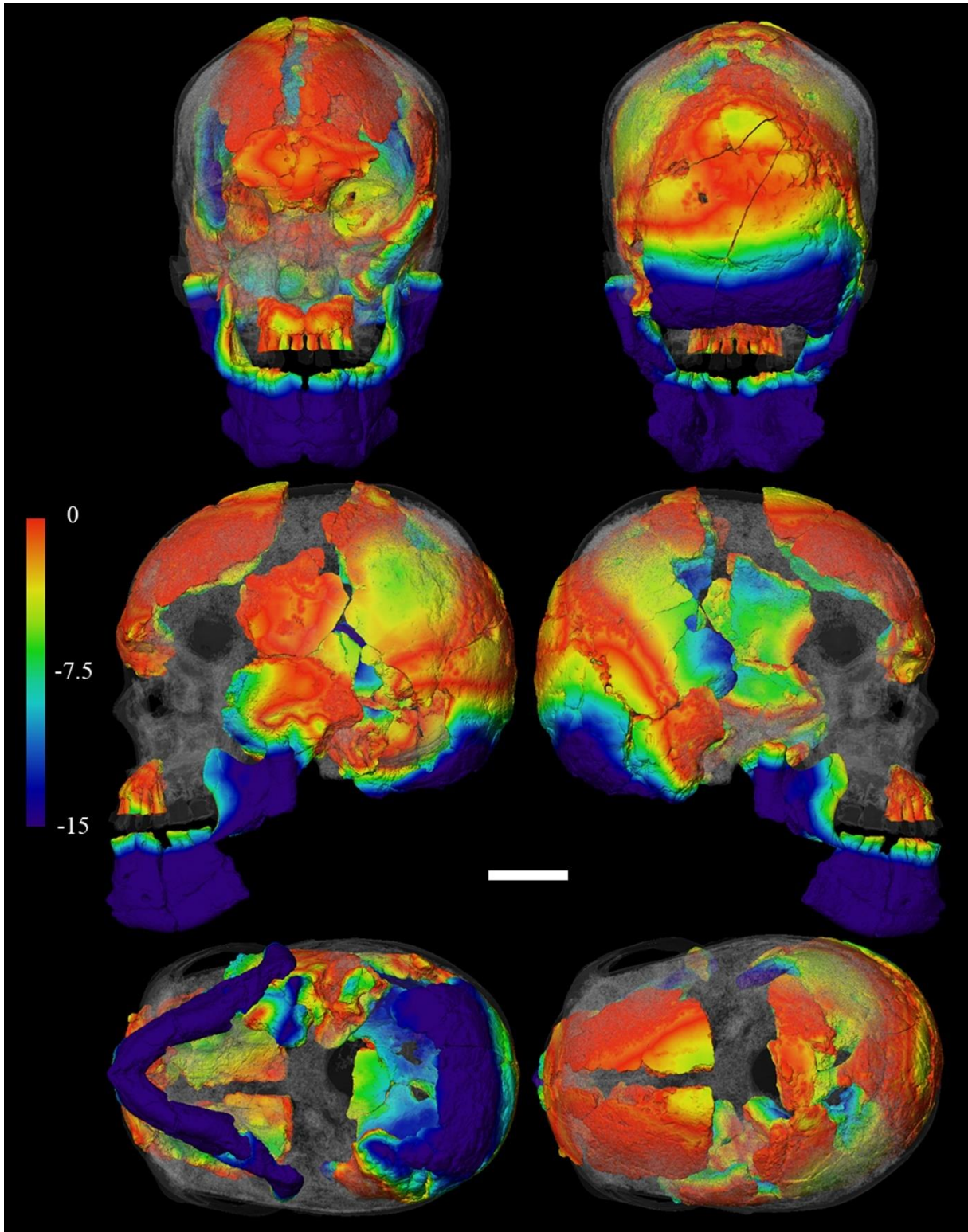
Figure 6. Surface displacement model of Kabua 1 reconstruction and Masai 03 as the reference (transparent). Scale of colormap: 0 – 15 mm deviation. Top-left: *norma frontalis*; top-right: *norma occipitalis*; center-left: *norma lateralis sinister*; center-right: *norma lateralis dexter*; bottom-left: *norma basilaris*; bottom-right: *norma verticalis* (scale bar = 5 cm).

In conclusion, the K1 material has presented us with a challenge, due to the incompleteness of the most diagnostically important areas, as well as the pronounced taphonomic distortion in the parieto-temporal region. Our reconstructions show that, even though direct articulation between several fragments is retained, the separate sections can be spatially manipulated with several degrees of freedom and still result in acceptable anatomical configurations. As such, the reference-based approach was useful in limiting the spatial distribution of the fragments with respect to each other and to the reference specimen.

To return to the results presented in this manuscript, we found that, in general, the K1 cranium exhibits a globular neurocranium and relatively gracile features, without substantial evidence for plesiomorphic traits, such as a sharp occipital angle, a low and sloping frontal bone, and pronounced supra-orbital and occipital tori. Thus, in this regard, we tentatively agree with Rightmire (1975), Bräuer (1978), and Schepartz (1987) that the K1 cranium is within the range of anatomically *H. sapiens* variation. This hypothesis is strengthened by the fact that it was quite difficult to fit these fragments with reference to pre-modern specimens without violating basic anatomical principles. The findings presented in this manuscript stand in contrast with the proposed 'Neanderthaloid' affinities put forth by Whitworth (1966) for the Kabua material. However, his hypothesis should be viewed within the context of the knowledge of human evolution at the time of its initial description. We have the benefit of working with a more abundant fossil record, a wealth of knowledge generated in the last decades, and sophisticated technology that allowed us to investigate this fossil in minute detail. In addition, we were able to explore multiple scenarios without the potential dangers involved in handling these delicate materials.

Outstanding questions on this material include the phylogenetic affinities of the Kabua 1 specimen, as well as the antiquity of both assemblages. This manuscript has presented the first steps towards evaluating its taxonomic affiliation by investigating the preserved qualitative traits. Moreover, the anatomical reconstructions described here will be used for geometric morphometric analyses of the Kabua material in order to determine the taxonomic affiliation of this specimen and its place in the African fossil record. Finally, the Kabua skeletal assemblages contain a wealth of other information that should now be more widely incorporated in the context of human evolution for years to come.

Acknowledgements

References

Ajmani, M. L., R. K. Mittal, and S. P. Jain. 1983. Incidence of the Metopic Suture in Adult Nigerian Skulls. Journal of Anatomy 137: 177-83.

Ambrose, S. H. 1980. Elmenteitan and Other Late Pastoral Neolithic Adaptations in the Central Highlands of East Africa. Proceedings of the 8th Panafrican Congress of Prehistory and Quaternary Studies, 1977, Nairobi.

Balzeau, A., L. T. Buck, L. Albessard, G. Becam, D. Grimaud-Hervé, T. C. Rae, and C. B. Stringer. 2017. The Internal Cranial Anatomy of the Middle Pleistocene Broken Hill 1 Cranium. Paleoanthropology 2017: 107-38.

Balzeau, A., and H. Rougier. 2010. Is the Suprainiac Fossa a Neandertal Autapomorphy? A Complementary External and Internal Investigation. Journal of Human Evolution 58: 1-22.

Blegen N, Faith JT, Mant-Melville A, Peppe DJ, Tryon CA. The Middle Stone Age after 50,000 years ago: New evidence from the Late Pleistocene sediments of the Eastern Lake Victoria Basin, Western Kenya. PaleoAnthropology. 2017;2017:139–69.

Brace, C. L. 1979. Krapina, "Classic" Neanderthals, and the Evolution of the European Face. Journal of Human Evolution 8: 527-50.

Bräuer, G. 1978. The Morphological Differentiation of Anatomically Modern Man in Africa, with Special Regard to Recent Finds from East Africa. Zeitschrift für Morphologie und Anthropologie 69: 266-92.

Bräuer, G. 1983. Die Menschlichen Skelettfunde Des" Later Stone Age" Aus Der Mumba-Höhle Und Anderen Lokalitäten Nahe Des Eyasi-Sees (Tanzania) Und Ihre Bedeutung Für Die Populationsdifferenzierung in Ostafrika. In Die Archäologischen Und Anthropologischen Ergebnisse Der Kohl-Larsen-Expeditionen in Nord-Tanzania, 1933–1939, edited. by H. Müller-Beck. Tübingen: Verlag Archaeologica Venatoria.

Bräuer, G. 2008. The Origin of Modern Anatomy: By Speciation or Intraspecific Evolution? Evolutionary Anthropology: Issues, News, and Reviews 17: 22-37.

Buck, L. T., and C. B. Stringer. 2015. A Rich Locality in South Kensington: The Fossil Hominin Collection of the Natural History Museum, London. Geological Journal 50: 321-37.

Buikstra, J. E., and D. H. Ubelaker. 1994. Standards for Data Collection from Human Skeletal Remains. Fayetteville, Arkansas: Arkansas Archaeological Survey Report Number 44.

Crevecoeur, I., A. Brooks, I. Ribot, E. Cornelissen, and P. Semal. 2016. Late Stone Age Human Remains from Ishango (Democratic Republic of Congo): New Insights on Late Pleistocene Modern human diversity in Africa. Journal of Human Evolution 96: 35-57.

Crevecoeur, I., H. Rougier, F. Grine, and A. Froment. 2009. Modern Human Cranial Diversity in the Late Pleistocene of Africa and Eurasia: Evidence from Nazlet Khater, Peştera Cu Oase, and Hofmeyr. American Journal of Physical Anthropology 140: 347-58.

Day, M. H., M. D. Leakey, and C. Magori. 1980. A New Hominid Fossil Skull (L.H. 18) from the Ngaloba Beds, Laetoli, Northern Tanzania. Nature 284: 55-6.

Deino, A. L., A. K. Behrensmeyer, A. S. Brooks, J. E. Yellen, W. D. Sharp, and R. Potts. 2018. Chronology of the Acheulean to Middle Stone Age Transition in Eastern Africa. Science 360: 95-8.

Fleagle, J. G., Z. Assefa, F. H. Brown, and J. J. Shea. 2008. Paleoanthropology of the Kibish Formation, Southern Ethiopia: Introduction. Journal of Human Evolution 55: 360-5.

Franciscus, R. G., and E. Trinkaus. 1995. Determinants of Retromolar Space Presence in Pleistocene Homo Mandibles. Journal of Human Evolution 28: 577-95.

Freidline, S. E., P. Gunz, K. Harvati, and J.-J. Hublin. 2012. Middle Pleistocene Human Facial Morphology in an Evolutionary and Developmental Context. Journal of Human Evolution 63: 723-40.

Fuchs, V. E. 1934. The Geological Work of the Cambridge Expedition to the East African Lakes, 1930–31. Geological Magazine 71: 97-112.

Grine, F. E., R. M. Bailey, K. Harvati, R. P. Nathan, A. G. Morris, G. M. Henderson, I. Ribot, and A. W. Pike. 2007. Late Pleistocene Human Skull from Hofmeyr, South Africa, and Modern Human Origins. Science 315: 226-9.

Grün, R., C. Stringer, F. McDermott, R. Nathan, N. Porat, S. Robertson, L. Taylor, G. Mortimer, S. Eggins, and M. McCulloch. 2005. U-Series and ESR Analyses of Bones and Teeth Relating to the Human Burials from Skhul. Journal of Human Evolution 49: 316-34.

Gunz, P., P. Mitteroecker, S. Neubauer, G. W. Weber, and F. L. Bookstein. 2009. Principles for the Virtual Reconstruction of Hominin Crania. Journal of Human Evolution 57: 48-62.

Gunz, P., S. Neubauer, L. Golovanova, V. Doronichev, B. Maureille, and J.-J. Hublin. 2012. A Uniquely Modern Human Pattern of Endocranial Development. Insights from a New Cranial Reconstruction of the Neandertal Newborn from Mezmaiskaya. Journal of Human Evolution 62: 300-13.

Harvati, K. 2015. Neanderthals and Their Contemporaries. In Handbook of Paleoanthropology, edited. by W. Henke and I. Tattersall, pp. 2243-2279. New York: Springer.

Harvati, K., P. Gunz, and D. Grigorescu. 2007. Cioclovina (Romania): Affinities of an Early Modern European. Journal of Human Evolution 53: 732-46.

Harvati, K., C. Stringer, R. Grün, M. Aubert, P. Allsworth-Jones, and C. A. Folorunso. 2011. The Later Stone Age Calvaria from Iwo Eleru, Nigeria: Morphology and Chronology. PloS One 6: e24024.

Hay, R. L. 1987. Geology of the Laetoli Area. In Laetoli: A Pliocene Site in Northern Tanzania, edited by M. D. Leakey and J. M. Harris, 23-47. Oxford: Oxford University Press.

Hublin, J.-J. 1978. Quelques Caractères Apomorphes Du Crâne Néandertalien Et Leur Interprétation Phylogénique. Comptes rendus de l'Académie des sciences. Série III, Sciences de la vie. D287: 923-6.

Hublin, J. -J. 2009. The origin of Neandertals. Proceedings of the National Academy of Sciences 106(38): 16022-7.

Hublin, J.-J., A. Ben-Ncer, S. E. Bailey, S. E. Freidline, S. Neubauer, M. M. Skinner, I. Bergmann, A. Le Cabec, S. Benazzi, K. Harvati, and P. Gunz. 2017. New Fossils from Jebel Irhoud, Morocco and the Pan-African Origin of Homo Sapiens. Nature 546: 289-92.

Hrdlička, A. 1927. The Neanderthal Phase of Man. The Journal of the Royal Anthropological Institute of Great Britain and Ireland 57, 249-74.

Kupczik, K., and J.-J. Hublin. 2010. Mandibular Molar Root Morphology in Neanderthals and Late Pleistocene and Recent Homo Sapiens. Journal of Human Evolution 59: 525-41.

Mehlman, M. J. 1979. Mumba-Hohle Revisited: The Relevance of a Forgotten Excavation to Some Current Issues in East African Prehistory. World Archaeology 11: 80-94.

Millard, A. R. 2008. A Critique of the Chronometric Evidence for Hominid Fossils: I. Africa and the near East 500–50ka. Journal of Human Evolution 54: 848-74.

Mitteroecker, P., P. Gunz, M. Bernhard, K. Schaefer, and F. L. Bookstein. 2004. Comparison of Cranial Ontogenetic Trajectories among Great Apes and Humans. Journal of Human Evolution 46: 679-98.

Mitteroecker, P., P. Gunz, S. Windhager, and K. Schaefer. 2013. A Brief Review of Shape, Form, and Allometry in Geometric Morphometrics, with Applications to Human Facial Morphology. Hystrix, the Italian Journal of Mammalogy 24: 8.

Morgan, L. E., and P. R. Renne. 2008. Diachronous Dawn of Africa's Middle Stone Age: New 40Ar/39Ar Ages from the Ethiopian Rift. Geology 36: 967-70.

Neubauer, S., J.-J. Hublin, and P. Gunz. 2018. The Evolution of Modern Human Brain Shape. Science Advances 4.

Nicholson, E., and K. Harvati. 2006. Quantitative Analysis of Human Mandibular Shape Using Three-Dimensional Geometric Morphometrics. American Journal of Physical Anthropology 131: 368-83.

Owen, R. B., J. W. Barthelme, R. W. Renaut, and A. Vincens. 1982. Palaeolimnology and Archaeology of Holocene Deposits North-East of Lake Turkana, Kenya. Nature 298: 523-9.

Pearson, O. M. 2008. Statistical and Biological Definitions of "Anatomically Modern" Humans: Suggestions for a Unified Approach to Modern Morphology. Evolutionary Anthropology: Issues, News, and Reviews 17: 38-48.

Phenice, T. W. 1972. Hominid Fossils: An Illustrated Key. Iowa: W. C. Brown Co.

Rak, Y. 1986. The Neanderthal: A New Look at an Old Face. Journal of Human Evolution 15: 151-64.

Reyes-Centeno, H., L. T. Buck, C. Stringer, and K. Harvati. 2014. The Inner Ear of the Eyasi I (Tanzania) and Kauba I (Kenya) Hominin Fossils. The African Human Fossil Record, Toulouse, 26-27 September.

Rightmire, G. P. 1975. Problems in the Study of Later Pleistocene Man in Africa. American Anthropologist 77: 28-52.

Robbins, L. 1972. Archeology in the Turkana District, Kenya. Science 176: 359-66.

Rosas, A. 2001. Occurrence of Neanderthal Features in Mandibles from the Atapuerca-Sh Site. American Journal of Physical Anthropology 114: 74-91.

Rosas, A., and M. Bastir. 2004. Geometric Morphometric Analysis of Allometric Variation in the Mandibular Morphology of the Hominids of Atapuerca, Sima De Los Huesos Site. The Anatomical Record Part A: Discoveries in Molecular, Cellular, and Evolutionary Biology 278A: 551-60.

Sahle, Y., W. K. Hutchings, D. R. Braun, J. C. Sealy, L. E. Morgan, A. Negash, and B. Atnafu. 2013. Earliest Stone-Tipped Projectiles from the Ethiopian Rift Date to >279,000 Years Ago. PLOS ONE 8: e78092.

Santa Luca, A. P. 1978. A Re-Examination of Presumed Neandertal-Like Fossils. Journal of Human Evolution 7: 619-36.

Schepartz, L. A. 1987. From Hunters to Herders: Subsistence Pattern and Morphological Change in Eastern Africa. Ph.D., Anthropology, University of Michigan.

Shea, J. J., and E. A. Hildebrand. 2010. The Middle Stone Age of West Turkana, Kenya. Journal of Field Archaeology 35: 355-64.

Smith, F. H., and G. C. Ranyard. 1980. Evolution of the Supraorbital Region in Upper Pleistocene Fossil Hominids from South-Central Europe. American Journal of Physical Anthropology 53: 589-610.

Stringer, C. 2016. The Origin and Evolution of Homo Sapiens. Philosophical Transactions of the Royal Society B: Biological Sciences 371.

Stringer, C. B., J.-J. Hublin, and B. Vandermeersch. 1984. The Origin of Anatomically Modern Humans in Western Europe. In The Origins of Modern Humans: A World Survey of the Fossil Evidences, edited. by H Smith and F Spencer, 51-135. New York: Alan R. Liss.

Tribolo, C., Asrat, A., Bahain, J.-J., Chapon, C., Douville, E., Fragnol, C., Hernandez, M., Hovers, E., Leplongeon, A., and Martin, L. 2017. Across the gap: geochronological and sedimentological analyses from the Late Pleistocene-Holocene sequence of Goda Buticha, southeastern Ethiopia. PloS One 12, e0169418.

Tryon, C. A., I. Crevecoeur, J. T. Faith, R. Ekshtain, J. Nivens, D. Patterson, E. N. Mbua, and F. Spoor. 2015. Late Pleistocene Age and Archaeological Context for the Hominin Calvaria from Gvjm-22 (Lukenya Hill, Kenya). Proceedings of the National Academy of Sciences 112: 2682-7.

Weber, G. W. 2001. Virtual Anthropology (Va): A Call for Glasnost in Paleoanthropology. The Anatomical Record 265: 193-201.

Weber, G. W. 2015. Virtual Anthropology. American Journal of Physical Anthropology 156: 22-42.

Weber, G. W., and F. L. Bookstein. 2011. Virtual Anthropology: A Guide to a New Interdisciplinary Field. Vienna/New York: Springer.

White, T. D., B. Asfaw, D. DeGusta, H. Gilbert, G. D. Richards, G. Suwa, and F. Clark Howell. 2003. Pleistocene Homo Sapiens from Middle Awash, Ethiopia. Nature 423: 742-7.

Whitworth, T. 1960. Fossilized Human Remains from Northern Kenya. Nature 185: 947-8.

Whitworth, T. 1965a. Artifacts from Turkana, Northern Kenya. The South African Archaeological Bulletin 20: 75-8.

Whitworth, T. 1965b. The Pleistocene Lake Beds of Kabua, Northern Kenya. Durham University Journal 57: 88-100.

Whitworth, T. 1966. A Fossil Hominid from Rudolf. The South African Archaeological Bulletin 21: 138-50.

Wilshaw, A. 2016. The Current Status of the Kenya Capsian. The African Archaeological Review 33: 13-27.

Wood, B. A. 2011. Wiley-Blackwell Encyclopedia of Human Evolution. Oxford, UK: Blackwell.

Zdilla, M. J., M. L. Russell, A. W. Koons, K. N. Bliss, and K. R. Mangus. 2018. Metopism: A Study of the Persistent Metopic Suture. Journal of Craniofacial Surgery 29: 204-8.

Zollikofer, C. P., and M. S. Ponce de León. 2005. Virtual Reconstruction: A Primer in Computer-Assisted Paleontology and Biomedicine: Wiley-Interscience.

Zollikofer, C. P. E., M. S. Ponce De León, and R. D. Martin. 1998. Computer-Assisted Paleoanthropology. Evolutionary Anthropology: Issues, News, and Reviews 6: 41-54.

The Kabua 1 cranium: a virtual anatomical reconstruction

Supplemental Material

Supplementary Tables

Supplementary Table 1: Kabua 1 fragments and their corresponding indices. Four fragments, here designated as Un-900 to Un-903, were too small to be identified securely and were thus not incorporated in the reconstructions. Fragments grouped under EM2471 have been described here but were not included in the reconstructions (see text).

| Number	Description
EM2468_01	This fragment is composed of both parietals, as it lies on the sagittal plane, located some distance posterior of bregma. There is slight taphonomic damage on the anterior and posterior portions. Articulates with EM2468_02 and EM2468_13.
EM2468_02	Fragment composed of the posterior right parietal and superolateral right of the occipital bone. Its occipital part consists of both the *planum occipitale*, and the *planum nuchale*. The parietal and occipital parts are separated by the lambdoidal suture, which is expanded due to taphonomic influence and resembles a large fissure. The fragment shows extensive degradation of the external table and multiple circular or semicircular cavities. A true perforation is present in the middle of the lambdoidal suture. Anatomical characteristics include internal occipital protuberance, part of the cruciform eminence, part of the nuchal torus, and superior nuchal lines. Articulates with EM2468_01 to EM2468_08, and EM2468_10.
EM2468_03	Rectangular parietal fragment, positioned anteromedially. This fragment is glued on the ectocranial surface of EM2468_04.
EM2468_04	Lateral right fragment of the *planum occipitale* and *planum nuchale*. The fragment extends towards asterion. Anatomical characteristics: lambdoidal suture and superior nuchal lines. Articulates with EM2468_02, EM2468_03, EM2468_05, EM2468_06, and EM2468_07.
EM2468_05	Lateral right parietal fragment, located inferiorly and of endocranially EM2468_04 due to taphonomic distortion. Articulates with EM2468_04 and EM2468_05 but this articulation is distorted.
EM2468_06	Posterior portion of the right temporal bone. Anatomical characteristics: posteroinferior portion of supramastoid crest and mastoid process. Articulates with EM2468_03, EM2468_05, and EM2468_07.
EM2468_07	Small, triangular shaped, posterior fragment of the right portion of the *planum nuchale*. Articulates with EM2468_04.
EM2468_08	Large fragment that represents the left posterior portion of the left parietal, posterosuperior portion of the right parietal, and the occipital bone. It presents several small cavities and one large perforation, which is roughly 6 mm superior to inferior and 5 mm lateral to medial. Anatomical characteristics include the superior nuchal lines, lambdoidal

	suture, lambda, and the cruciform eminence. Articulates with EM2468_02, EM2468_09, and EM2468_10.
EM2468_09	Left inferolateral fragment of the *planum nuchale* of the occipital bone. Articulates with EM2468_08.
EM2468_10	This large fragment represents the superior part of the right parietal, left parietal and a small part of the occipital, although this is uncertain due to the absence of a clear lambdoidal suture on this side. Superomedially, there is a large, roughly triangular cavity (13 mm posteroanteriorly) where the outer layers of cranial bone gradually degrade. Anatomical characteristic: temporal line. Articulates with EM2468_01, EM2468_02, EM2468_08, EM2468_11, EM2468_12, EM2468_13, EM2470_18, and EM2470_20.
EM2468_11	Inferolateral fragment of left parietal. Located near the location of the parietomastoid suture. Slight erosion of external table. Articulates with EM2468_10 and EM2471_21
EM2468_12	Small fragment that belongs to the superolateral portion of the left parietal. Articulates with EM2468_10.
EM2468_13	Rounded parietal fragment, posterolateral left of bregma. Articulates with EM2468_10 and EM2468_01.
EM2469_14	Anteriorly positioned frontal fragment. Anatomical characteristics: supraorbital margin, superciliary arch, glabella, lacrimal fossa, and frontal crest. There is a large, likely taphonomic, break on the posterior medial portion, which starts as erosion of the external table and extends as a large fissure that separates EM2469_15 and EM2469_16 Articulates with EM2469_15, and EM2469_17.
EM2469_15	Right lateral, anterior frontal fragment. Forms the right portion of the frontal bone. Large presence of taphonomic fissure in the medial region.
EM2469_16	Right lateral posterior frontal fragment. There seems to be a very weak presence of the coronal suture. Articulates with EM2469_15 and EM2469_17.
EM2469_17	Left lateral frontal fragment. Forms the left portion of the frontal bone. Articulates with EM2469_14 and EM2469_16.
EM2470_18	Small triangular fragment, posterior portion of the left parietal. Articulates with EM2470_19.
EM2470_19	Lateral right parietal fragment. It is broken off around the coronal suture but there are no clear traces of this suture on this fragment. Anatomical characteristic: temporal line Articulates with EM2470_18, and EM2471_21.
EM2470_20	Small posterosuperior parietal fragment. Articulates with EM2468_10.
EM2470_21	Portion of the left temporal bone and inferior portion of the left parietal. Anatomical characteristics include the temporal squama and parietomastoid suture. Shows extensive erosion of the endocranial surface Articulates with EM2470_22, EM2470_23, EM2470_24, and EM2470_27.
EM2470_22	Small, rectangular, endocranial fragment of the left parietal bone. Articulates with EM2470_20.
EM2470_23	Inferior portion of left temporal squama. Expanded due to matrix in diploic layer. Articulates with EM2470_21, EM2470_24, and EM2470_27.

|	
EM2470_24	Anteroinferior fragment, base of the to the postglenoid process, located in between the superior and inferior fragments of the left squama. Articulates with EM2470_21, EM2470_23, EM2470_25, and EM2470_27.
EM2470_25	Posterosuperior part of the postglenoid process. Articulates with EM2470_24 and EM247026.
EM2470_26	Anteroinferior part of the postglenoid process and lateral part of the articular eminence. Articulates with EM2470_25.
EM2470_27	Petrous portion of the left temporal. Anatomical characteristics: internal auditory meatus, part of the mastoid process. Articulates with EM2470_21 and EM2470_23.
EM2471_28	Anterosuperior fragment of the right temporal squama, separated into two pieces but joined by sediment. Articulates with EM2471_35.
EM2471_29	Fragment of right temporal squama, protruding anteriorly from EM2471_35. Covered in sediment and separated into two pieces. Superior fragment.
EM2471_30	Fragment of right temporal squama, protruding anteriorly from EM2471_35. Covered in sediment and separated into two pieces. Inferior fragment. Does not articulate directly with EM2471_35.
EM2471_31	Lateral portion of right articular eminence. Articulates with EM2471_35.
EM2471_32	Separate endocranial fragment, medial of the right temporal squama. Articulates with EM2471_35.
EM2471_33	Part of the right sphenoid greater wing (?). Articulates with EM2471_34 and EM2471_35.
EM2471_34	Triangular fragment, anteroinferior endocranial. Articulates with EM2471_33 and EM2471_35.
EM2471_35	Body of the right temporal. Articulates with EM2471_28, EM2471_30, EM2471_31, EM2471_32, EM2471_33, and EM2471_34.
EM2481_36	Anterior fragment of the right maxilla. Retains the first upper incisor, the second upper incisor and the upper canine. Articulates with EM2481_37. Since the articulation seems to be perfect and presence of sediment minimal, this fragment was not segmented.
EM2481_37	Posterior fragment of the right maxilla. Retains P^3 and P^4. Articulates with EM2481_36. Was not segmented.
EM2480_38	Right hemimandible. Retains the second lower incisor, the first lower premolar, the second lower premolar, the second lower molar and the third lower molar. Anatomical characteristics include the upper ascending ramus, coronoid process, sigmoid notch, base of the mandibular condyles, and mandibular corpus. The pieces are not entirely separated, as there is still bone preserved between the middle portion and mandibular corpus and the mandibular ramus, as well as between the middle portion and the anterior part of the mandible. However, as can be seen in figure 1, most of the gonial angle and the area around the absent first molar have been glued and reconstructed.
Un-900	Small fragment of bone superior of EM2468_06.
Un-901	Small fragment inferior of the left parietal.
Un-902	Small fragment inferior of the left parietal.
Un-903	Very small fragment, located anteroinferior of the maxilla.

Supplementary Table 2: Morphological features described in the manuscript, and associated scores when applicable.

	Trait	**Buikstra & Ubelaker score (if applicable)**
Posterior calvaria	Laterally expressed superior nuchal lines	-
	Weakly expressed external occipital protuberance	1
	Weakly expressed cruciform eminence	-
	Shallow suprainiac depression	-
	No projection below lambda	-
	Parietal eminence	-
	Temporal line	-
Frontal	Sharp supraorbital margins	2
	Gracile glabella	1
	Discontinuous supraorbital tori	-
	Metopic suture	-
	Absence of post-toral sulcus	-
	Absence of postorbital constriction	-
	Minimal frontal keeling	-
Temporal	Small mastoid process	2
	Pronounced supramastoid crest	-
Mandible & Maxilla	Robust mylohyoid ridge	-
	Mandibular torus	-
	Deep mandibular corpus	-
	Mandibular symphysis (area not fully preserved)	-
	Possible retromolar gap	-
	Second and third lower molars with distinct roots	-
	Canine fossa (area not preserved)	-

Supplementary Figures
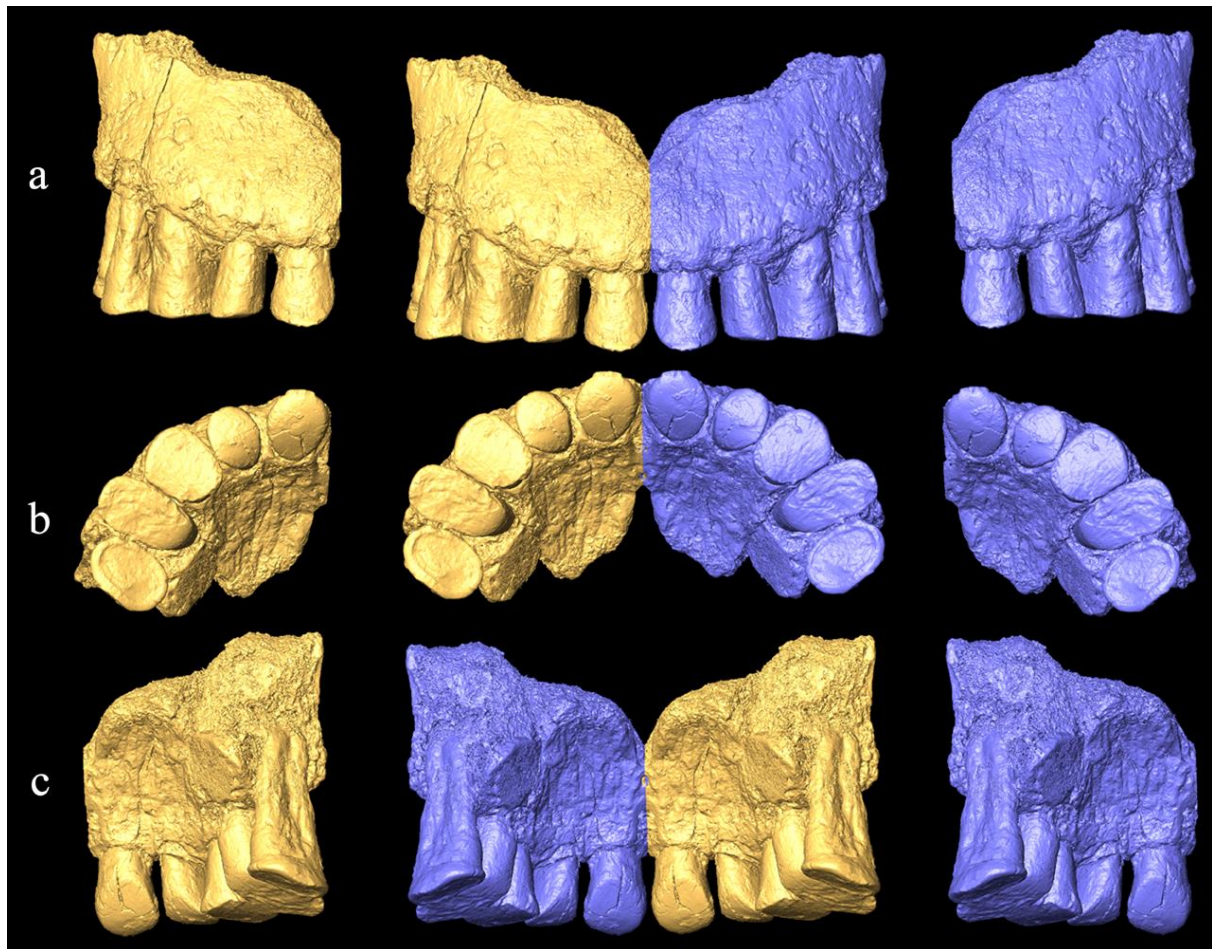
Supplementary Figure 1. Reconstruction of the dental arcade. Yellow: Original fragment, blue: reflection. Each row shows the original fragment, followed by the mirrored fragment and the reconstruction after aligning and merging the original with the mirrored counterpart. a) Labial view; b) ventral view; c) lingual view.
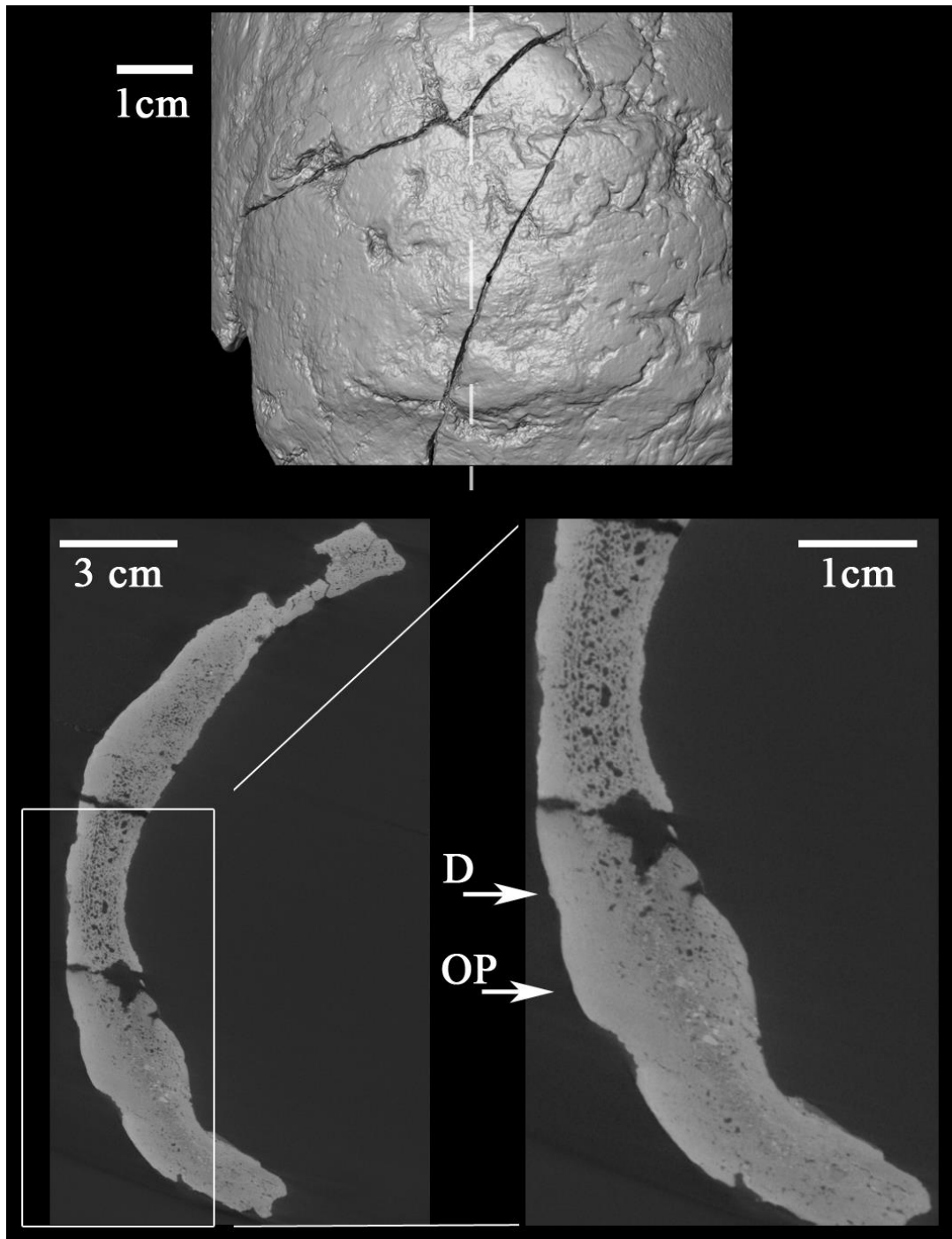
Supplementary Figure 2. Overview image of depression above inion on Kabua 1. Top: Zoom of Kabua 1 in *norma occipitalis*. Dashed line has been added to depict the location of the vertical slice. Bottom-left: Vertical slice through the Kabua 1 occipital bone. Bottom-right: Zoom on the vertical slice, showing the depression (D) and external occipital protuberance (OP) in detail.
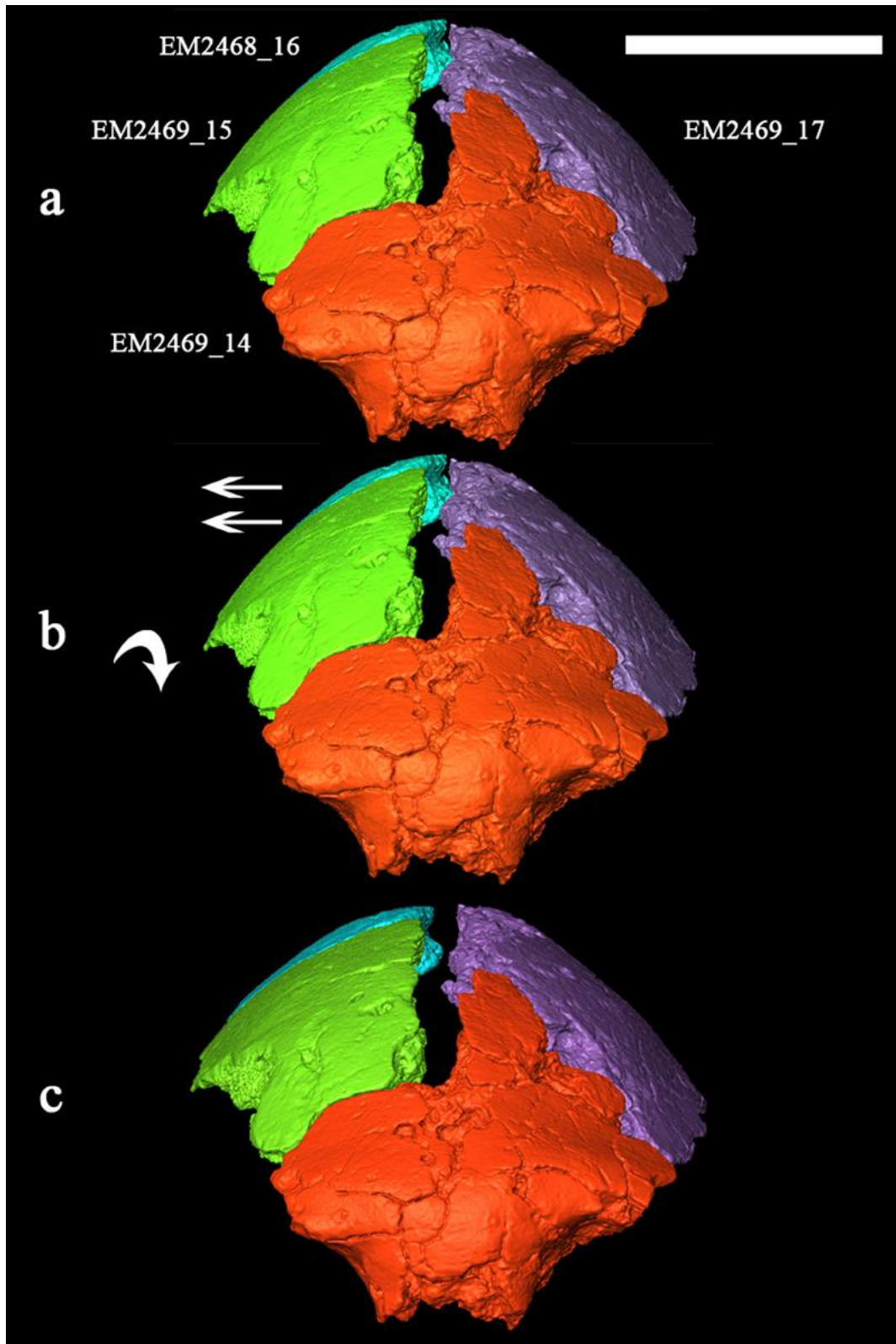
Supplementary Figure 3. Reconstruction of the anatomical articulation between the fragments of the frontal bone. a) Original position of fragments, segmented from the µCT scanned volume; b) Fragments EM2469_15 and EM2469_16 are rotated medially and subsequently moved laterally in order to achieve a better articulation between EM2469_14 and EM2469_15 (scale bar = 3 cm).
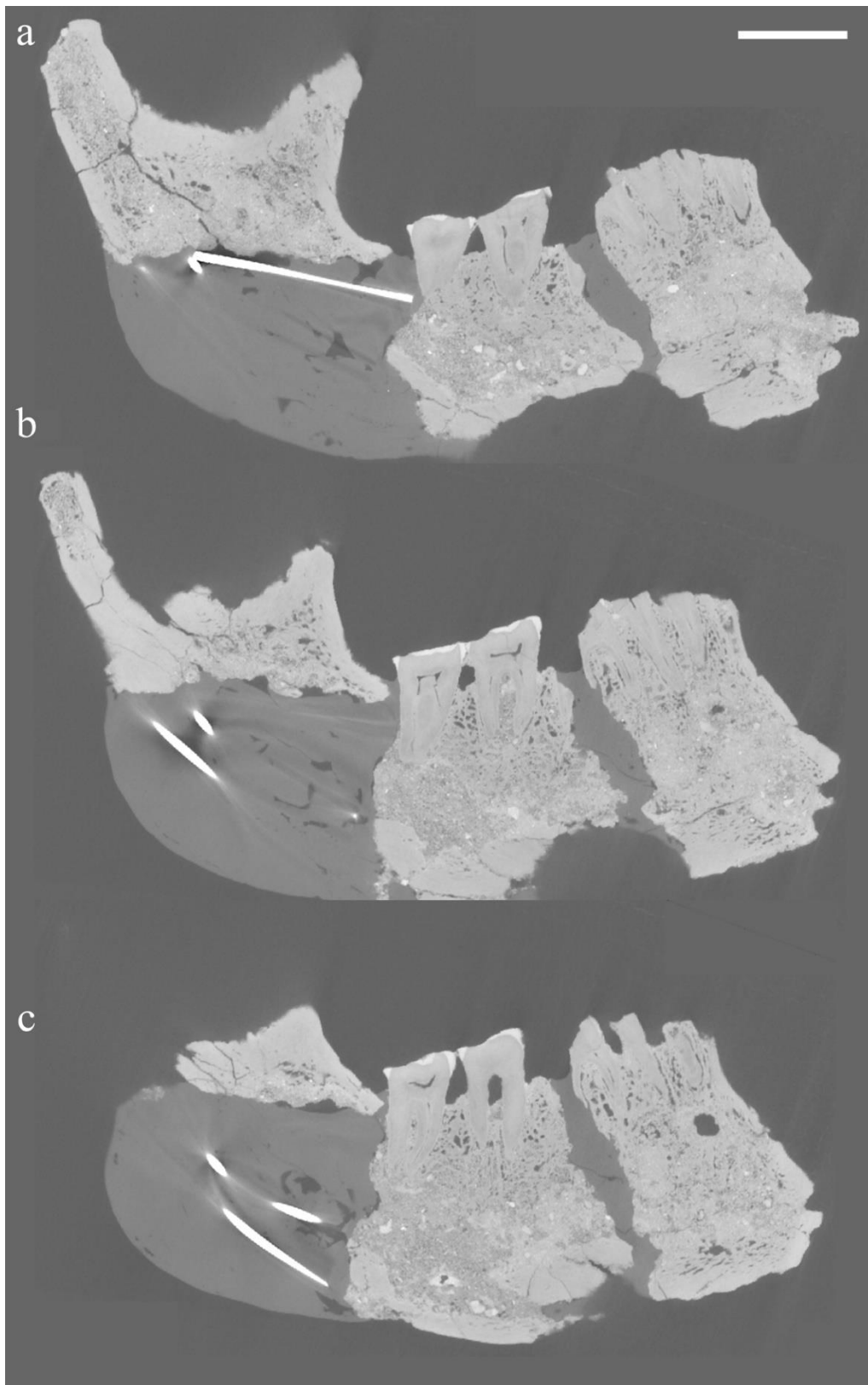
Supplementary Figure 4. Sequence of transverse CT slices through the mandible, buccal to lingual, showing the root morphology of M_2, and M_3. a) Lingual aspect of M_2, and M_3; b) middle of M_2, and M_3; c) buccal aspect of M_2, and M_3 (scale bar = 2 cm).
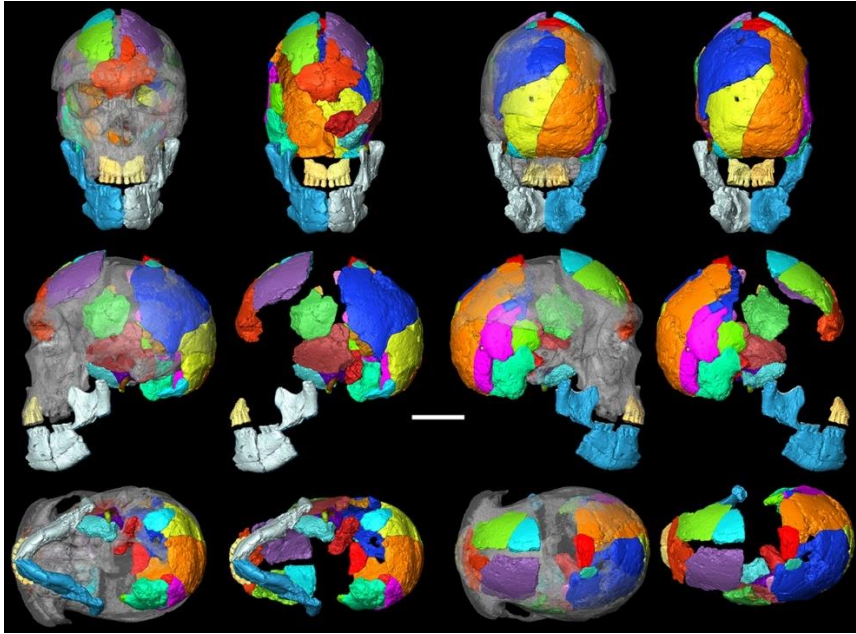
Supplementary Figure 5. Reconstruction of Kabua 1, with Broken Hill as the reference. Each pair of orientations shows the Kabua 1 material, either with or without Broken Hill transparent and superimposed. Top-left: *norma frontalis*; top-right: *norma occipitalis*; center-left: *norma lateralis sinister*; center-right: *norma lateralis dexter*; bottom-left: *norma basilaris*; bottom-right: *norma verticalis* (scale bar = 10 cm).
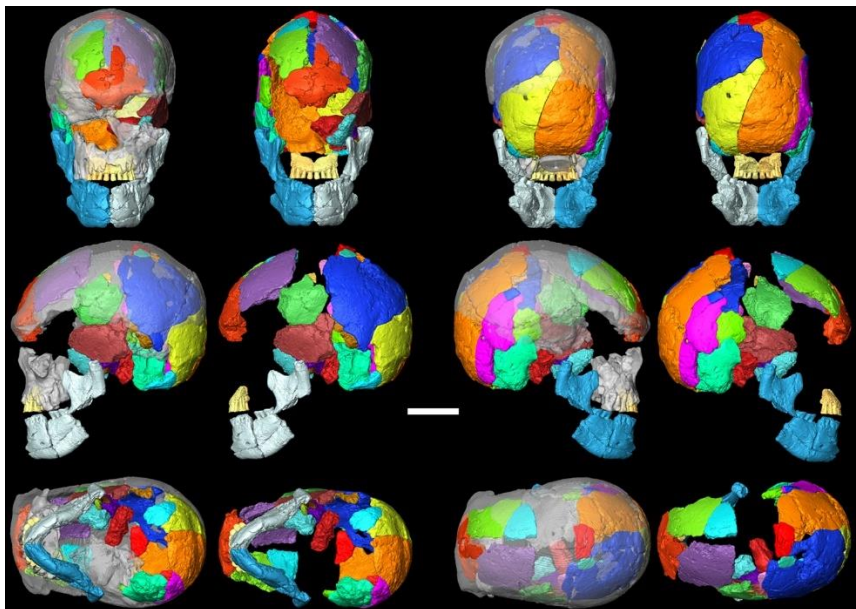

Supplementary Figure 6. Reconstruction of Kabua 1, with Ngaloba LH18 as the reference. Each pair of orientations shows the Kabua 1 material, both with and without Ngaloba LH18 transparent and superimposed. Top-left: *norma frontalis*; top-right: *norma occipitalis*; center-left: *norma lateralis sinister;* center-right: *norma lateralis dexter*; bottom-left: *norma basilaris*; bottom-right: *norma verticalis* (scale bar = 10 cm).

34
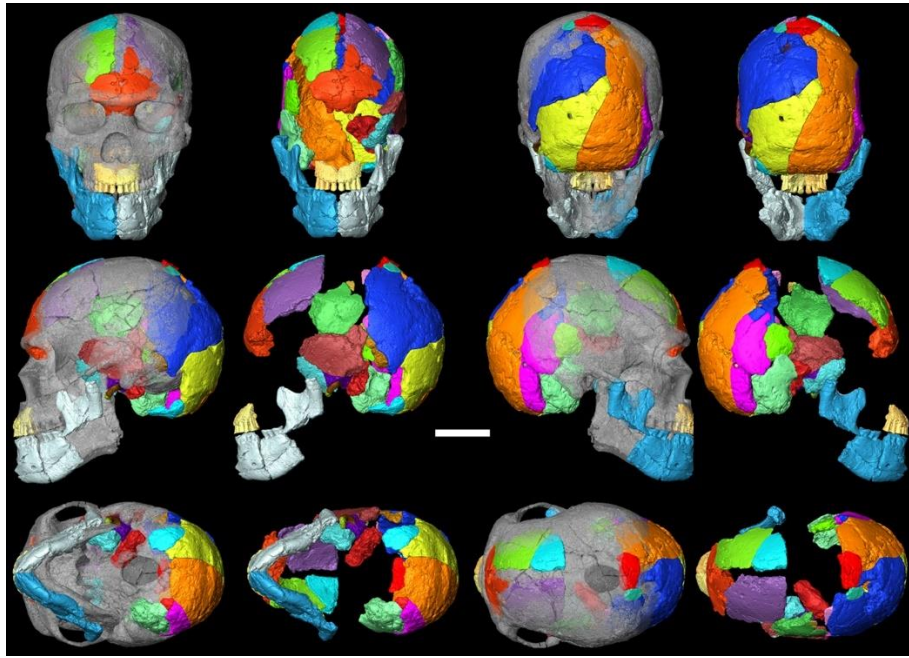
Supplementary Figure 7. Reconstruction of Kabua 1, with Skhūl V as the reference. Each pair of orientations shows the Kabua 1 material, both with and without Skhūl V transparent and superimposed. Top-left: *norma frontalis*; top-right: *norma occipitalis*; center-left: *norma lateralis sinister*; center-right: *norma lateralis dexter*; bottom-left: *norma basilaris*; bottom-right: *norma verticalis* (scale bar = 10 cm).
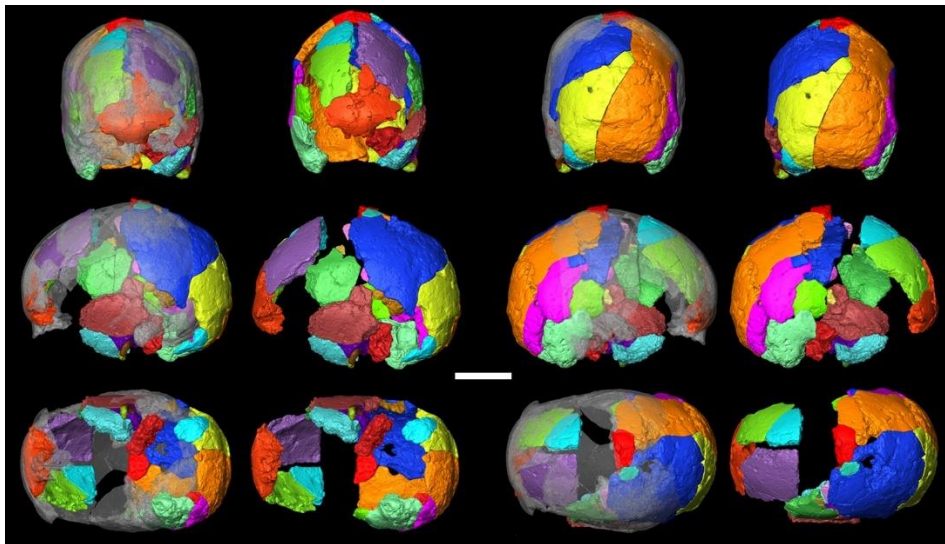

Supplementary Figure 8. Reconstruction of Kabua 1, with Mumba X as the reference. Each pair of orientations shows the Kabua 1 material, both with and without Mumba X transparent and superimposed. Top-left: *norma frontalis*; top-right: *norma occipitalis*; center-left: *norma lateralis sinister*; center-right: *norma lateralis dexter*; bottom-left: *norma basilaris*; bottom-right: *norma verticalis* (scale bar = 10 cm).
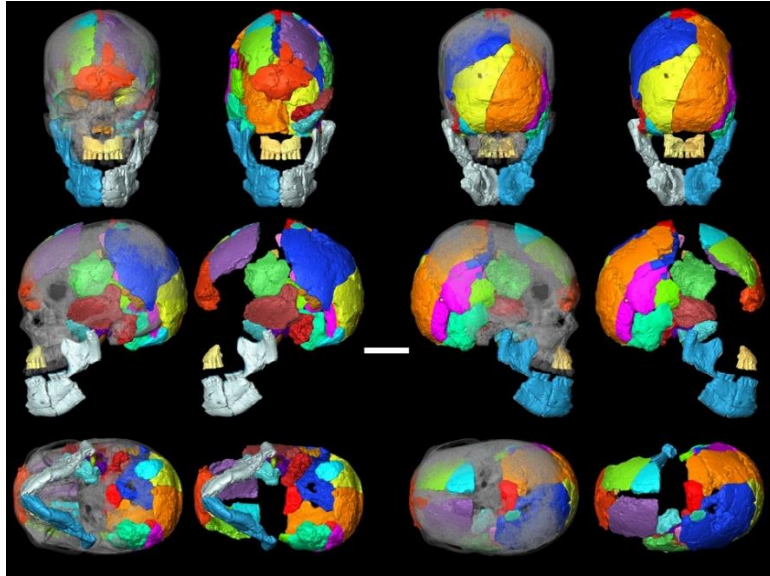
Supplementary Figure 9. Reconstruction of Kabua 1, with Masai 03 as the reference. Each pair of orientations shows the Kabua 1 material, both with and without Masai 03 transparent and superimposed. Top-left: *norma frontalis*; top-right: *norma occipitalis*; center-left: *norma lateralis sinister*; center-right: *norma lateralis dexter*; bottom-left: *norma basilaris*; bottom-right: *norma verticalis* (scale bar = 10 cm).
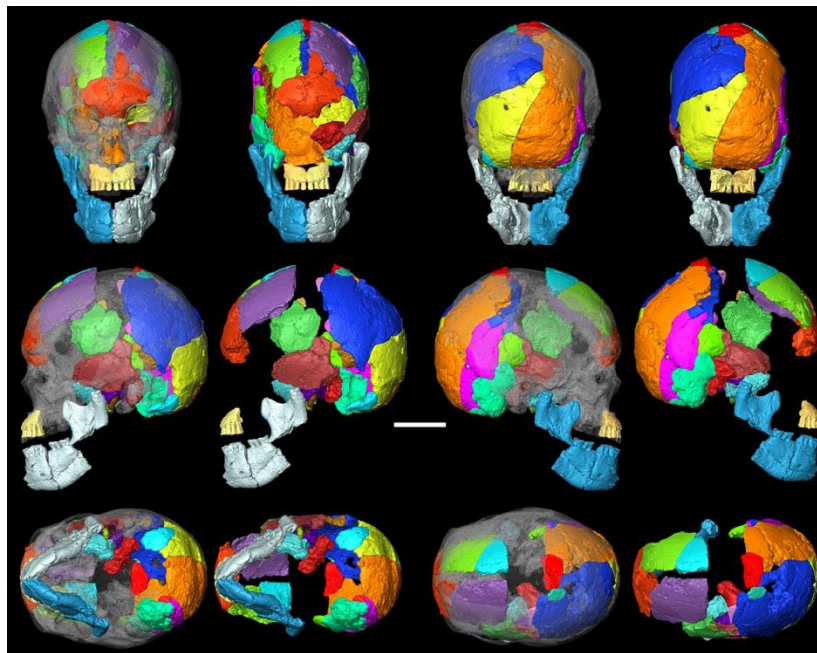

Supplementary Figure 10. Reconstruction of Kabua 1, with Masai 10 as the reference. Each pair of orientations shows the Kabua 1 material, both with and without Masai 10 transparent and superimposed. Top-left: *norma frontalis*; top-right: *norma occipitalis*; center-left: *norma lateralis sinister*; center-right: *norma lateralis dexter*; bottom-left: *norma basilaris*; bottom-right: *norma verticalis* (scale bar = 10 cm).
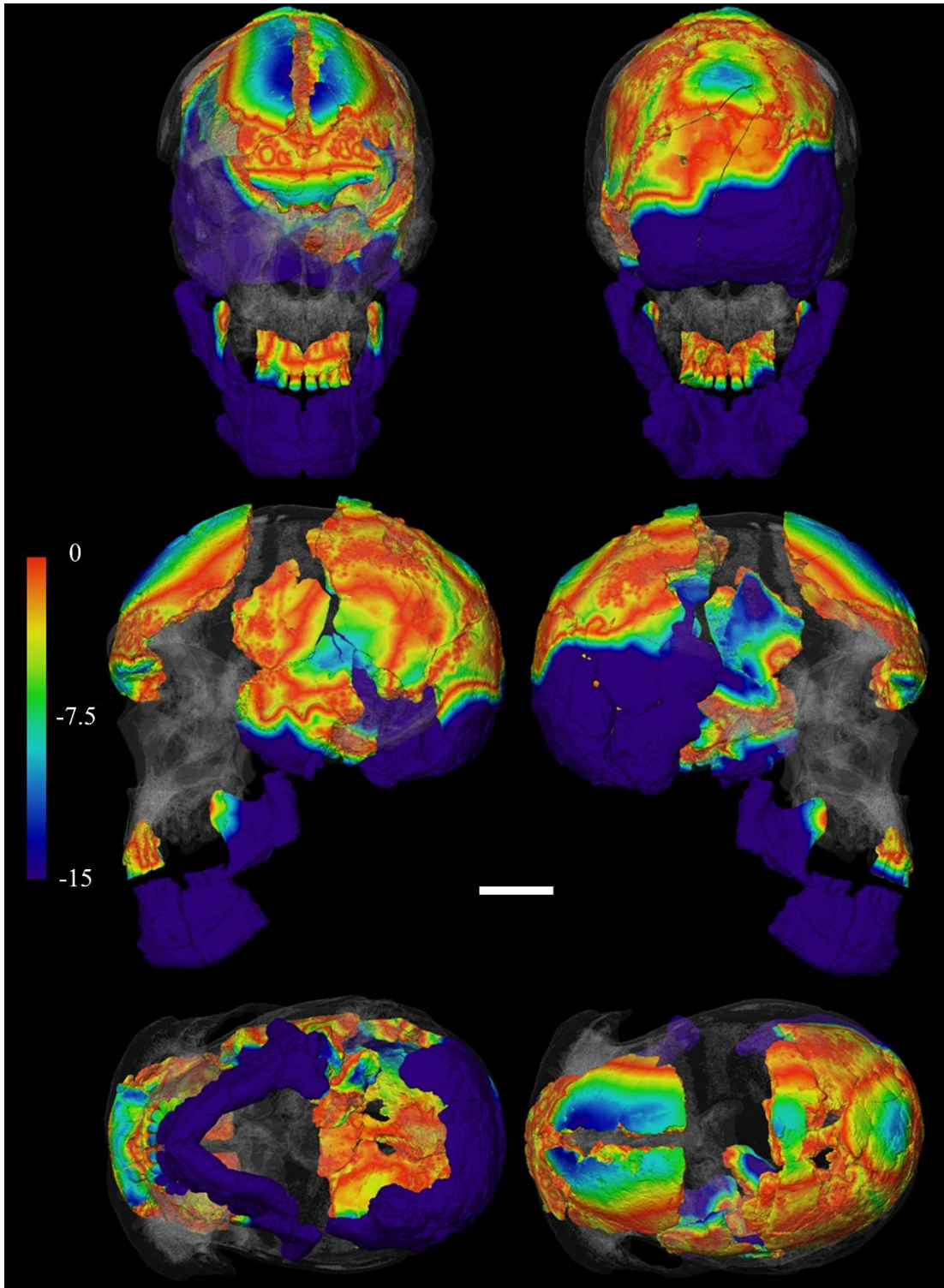
Supplementary Figure 11. Surface displacement model of Kabua 1 reconstruction and Broken Hill as the reference (transparent). Scale of colormap: 0 – 15 mm deviation. Top-left: *norma frontalis*; top-right: *norma occipitalis*; center-left: *norma lateralis sinister*; center-right: *norma lateralis dexter*; bottom-left: *norma basilaris*; bottom-right: *norma verticalis* (scale bar = 5 cm).
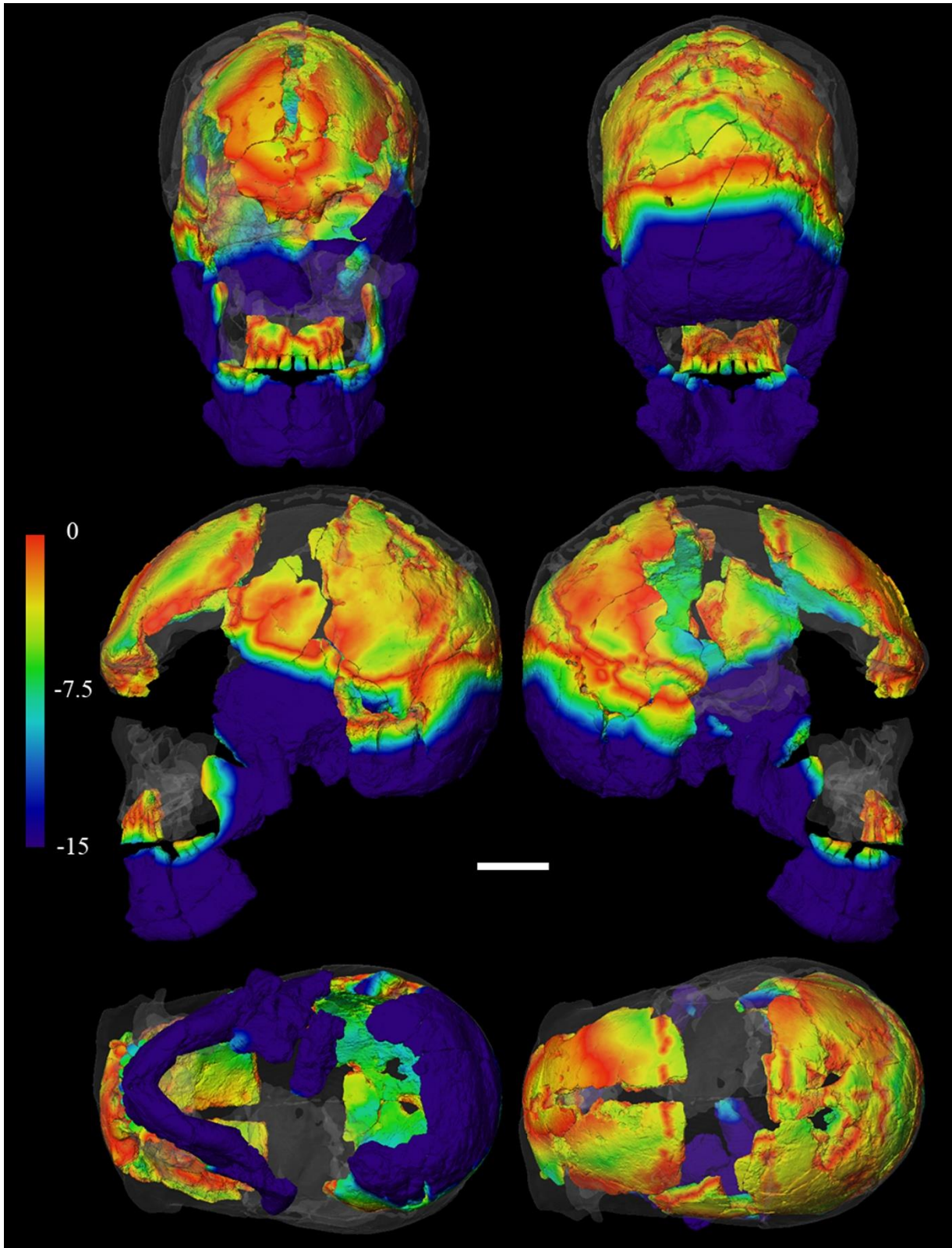
Supplementary Figure 12. Surface displacement model of Kabua 1 reconstruction and Ngaloba LH18 as the reference (transparent). Scale of colormap: 0 – 15 mm deviation. Top-left: *norma frontalis*; top-right: *norma occipitalis*; center-left: *norma lateralis sinister*; center-right: *norma lateralis dexter*; bottom-left: *norma basilaris*; bottom-right: *norma verticalis* (scale bar = 5 cm).
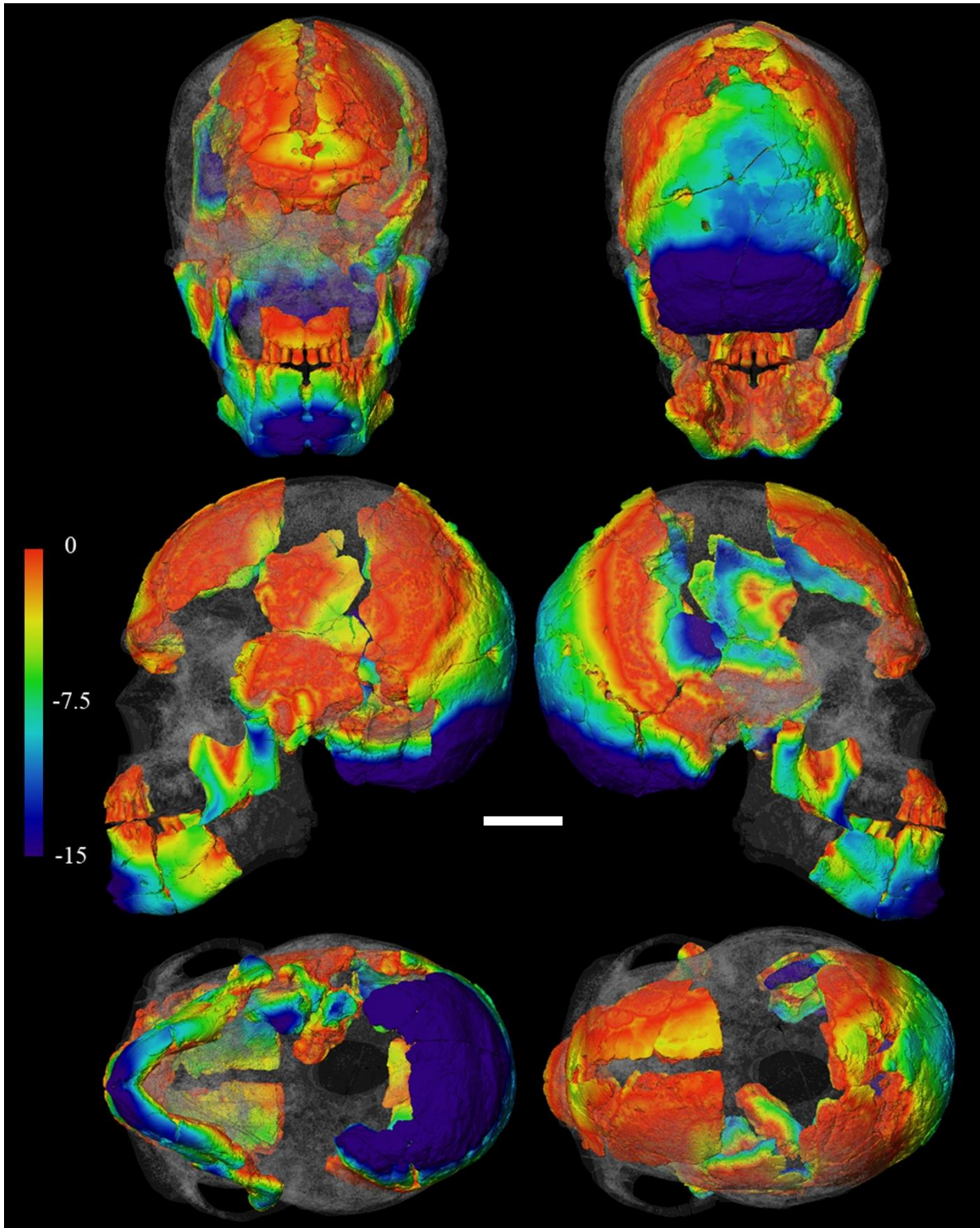
Supplementary Figure 13. Surface displacement model of Kabua 1 reconstruction and Skhūl V as the reference (transparent). Scale of colormap: 0 – 15 mm deviation. Top-left: *norma frontalis*; top-right: *norma occipitalis*; center-left: *norma lateralis sinister*; center-right: *norma lateralis dexter*; bottom-left: *norma basilaris*; bottom-right: *norma verticalis* (scale bar = 5 cm).
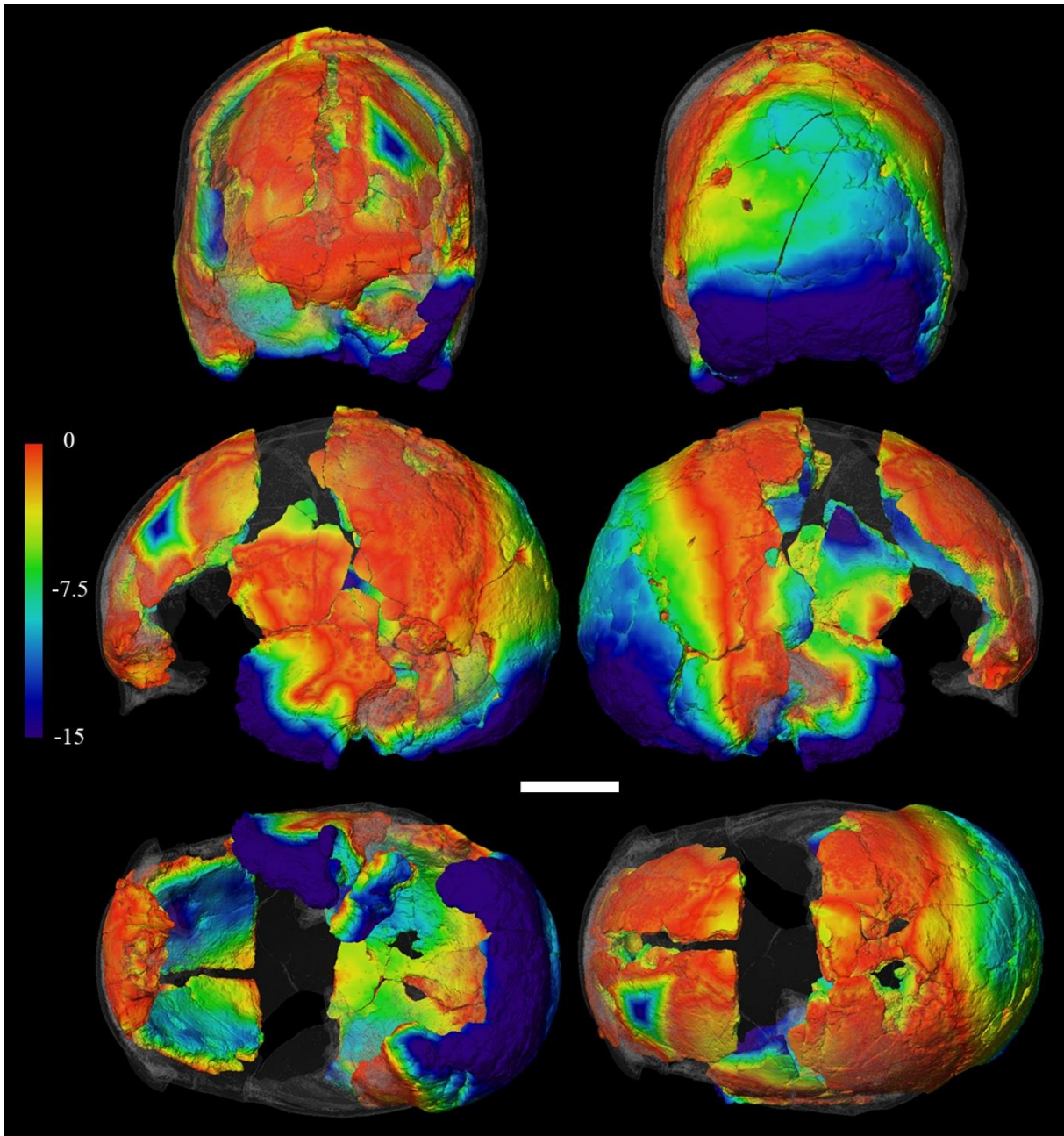
Supplementary Figure 14. Surface displacement model of Kabua 1 reconstruction and Mumba X as the reference (transparent). Scale of colormap: 0 – 15 mm deviation. Top-left: *norma frontalis*; top-right: *norma occipitalis*; center-left: *norma lateralis sinister*; center-right: *norma lateralis dexter*; bottom-left: *norma basilaris*; bottom-right: *norma verticalis* (scale bar = 5 cm).
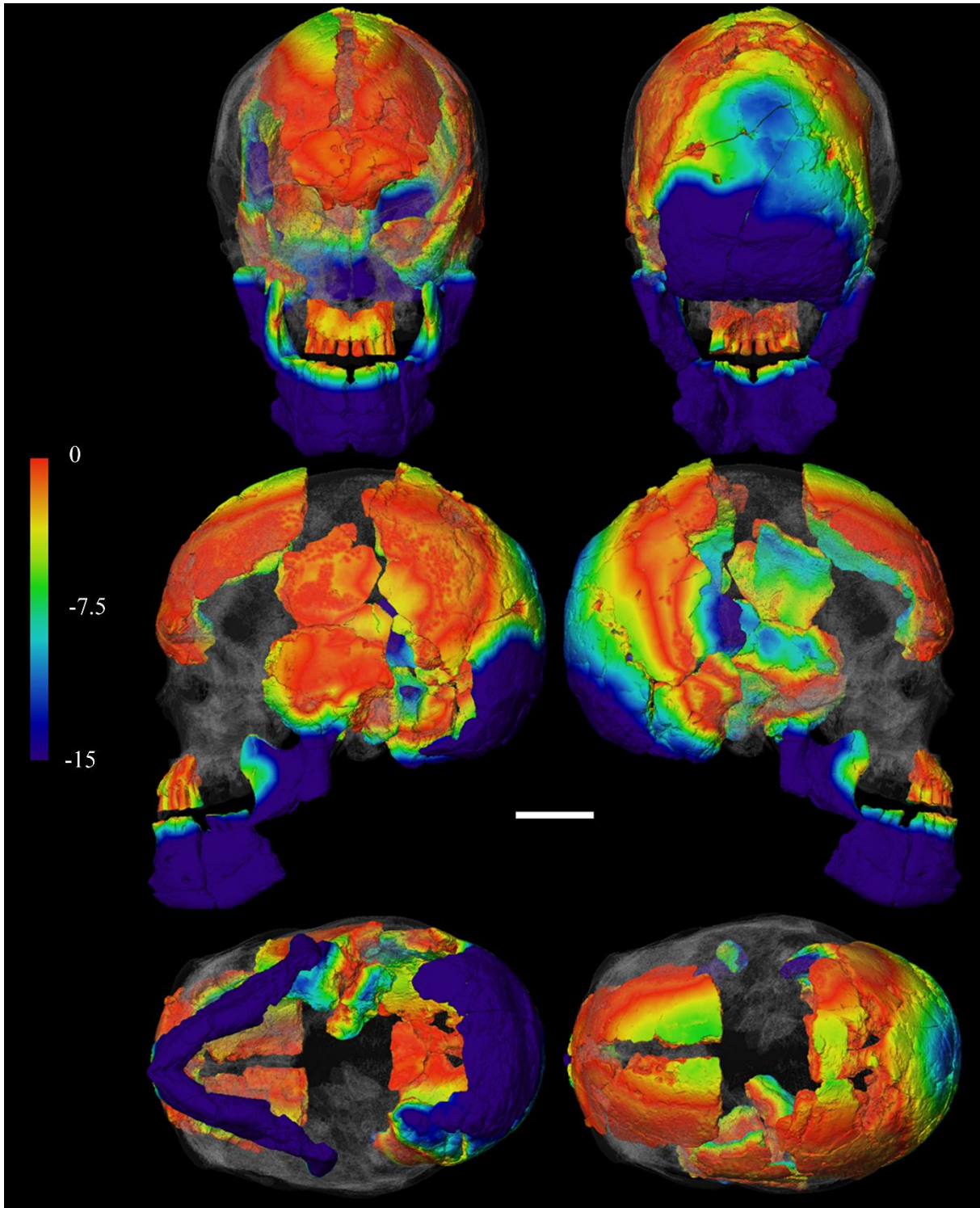
[SUPFIG15 here. Images of surfaces generated in Avizo Lite 9.0.1. Images rescaled and collated in Adobe Photoshop CS4 64 bit. Figure should be in color, RGB 8bit or CYMK]

Supplementary Figure 15. Surface displacement model of Kabua 1 reconstruction and Masai 10 as the reference (transparent). Scale of colormap: 0 – 15 mm deviation. Top-left: *norma frontalis*; top-right: *norma occipitalis*; center-left: *norma lateralis sinister*; center-right: *norma lateralis dexter*; bottom-left: *norma basilaris*; bottom-right: *norma verticalis* (scale bar = 5 cm).